Shipborne observations reveal contrasting Arctic marine, Arctic terrestrial and Pacific marine aerosol properties

Jiyeon Park[1], Manuel Dall'Osto[2], Kihong Park[3], Yeontae Gim[1], Hyo Jin Kang[1,4], Eunho Jang[1,4], Ki-Tae Park[1], Minsu Park[5], Seong Soo Yum[5], Jinyoung Jung[1], Bang Yong Lee[1], and Young Jun Yoon[1,*]

[1]Korea Polar Research Institute, 26 Songdomirae-ro, Yeonsu-gu, Incheon 21990, South Korea
[2]Institut de Ciències del Mar, CSIC, Pg. Marítim de la Barceloneta 37-49, 08003, Barcelona, Catalonia, Spain
[3]Gwangju Institute of Science and Technology (GIST), 123 Cheomdangwagi-ro, Buk-gu, Gwangju 61005, Republic of Korea
[4]University of Science and Technology (UST), 217 Gajeong-ro, Yuseong-gu, Daejeon, Republic of Korea
[5]Department of Atmospheric Sciences, Yonsei University, 50 Yonsei-ro, Seodaemun-gu, Seoul 03722, Korea

[*]*Correspondence to*: Y.J. Yoon (yjyoon@kopri.re.kr)

Abstract

There are few shipborne observations addressing the factors influencing the relationships of the formation and growth of aerosol particles with cloud condensation nuclei (CCN) in remote marine environments. In this study, the physical properties of aerosol particles throughout the Arctic Ocean and Pacific Ocean were measured aboard the Korean ice breaker R/V Araon during the summer of 2017 for 25 days. A number of New Particle Formation (NPF) events and growth were frequently observed in both Arctic terrestrial and Arctic marine air masses. By striking contrast, NPF events were not detected in Pacific marine air masses. Three major aerosol categories are therefore discussed: (1) Arctic marine (aerosol number concentration $CN_{2.5}$: 413 ± 442 cm^{-3}), (2) Arctic terrestrial ($CN_{2.5}$: 1622 ± 1450 cm^{-3}) and (3) Pacific marine ($CN_{2.5}$: 397 ± 185 cm^{-3}), following air mass back trajectory analysis. A major conclusion of this study is that not only that the Arctic Ocean is a major source of secondary aerosol formation relative to the Pacific Ocean; but also that open ocean sympagic and terrestrial influenced coastal ecosystems both contribute to shape aerosol size distributions. We suggest that terrestrial ecosystems - including river outflows and tundra - strongly affects aerosol emissions in the Arctic coastal areas, possibly more than anthropogenic Arctic emissions. The increased river discharge, tundra emissions and melting sea ice should be considered in future Arctic atmospheric composition and climate simulations. The average CCN concentrations at a supersaturation ratios of 0.4% were 35 ± 40 cm^{-3}, 71 ± 47 cm^{-3}, and 204 ± 87 cm^{-3} for Arctic marine, Arctic terrestrial, and Pacific marine aerosol

categories, respectively. Our results aim to help to evaluate how anthropogenic and natural atmospheric sources and processes affect the aerosol composition and cloud properties.

1. Introduction

The climate change experienced in the Arctic is more rapid than that occurring at mid-latitudes in a phenomenon known as Arctic amplification (ACIA, 2005). In the warming Arctic, the extent and thickness of sea-ice have dramatically decreased over the past few decades (Stroeve et al., 2012). It has been estimated that the Arctic may seasonally become sea ice-free Arctic in the next 30 years (Wang and Overland, 2009). Aerosol particles in the atmosphere are a major driver of the Arctic climate (IPCC, 2013), as they directly affect the climate through scattering and absorbing solar radiation (Stier et al., 2007), and indirectly by modifying the formation, properties, and lifetimes of clouds (Twomey, 1974). These direct and indirect effects are the leading uncertainty in current climate predictions. New particle formation (NPF), a predominant source of atmospheric particles, occurs through the formation of nanometer-sized molecular clusters (<~1 nm) (i.e., nucleation) and their subsequent growth into aerosol particles of a few nanometers (~1 – 10 nm) and larger (~>10 nm) (Kulmala et al., 2004; Zhang et al., 2012). NPF can significantly increase the number of aerosol particles in the atmosphere. During summer, the Arctic is more isolated from anthropogenic influences (Arctic Haze) and experiences comparatively pristine background aerosol conditions (Heintzenberg et al., 2015; Law and Stohl, 2007). As the number concentrations of particles in the Arctic during summer are very low (of an order of ~10^2 cm^{-3}) (Merikanto et al., 2009), the physicochemical properties of aerosol particles in the Arctic atmosphere is highly sensitive to NPF.

NPF events have been frequently observed within a wide range of environmental conditions at various Arctic locations, such as Zeppelin (Tunved et al., 2013; Croft et al., 2016; Heintzenberg et al., 2017), Tiksi (Asmi et al., 2016), Alert (Croft et al., 2016), Station Nord (Nguyen et al., 2016), and Barrow (Kolesar et al., 2017), and from limited ship-based observations (Chang et al., 2011; Kim et al., 2015; Heintzenberg et al., 2015). The formation and growth of particles in the Arctic atmosphere are

strongly influenced by marine, coastal, marginal ice, and/or anthropogenic sources. Oceanic dimethyl sulfide (DMS) and other volatile organic precursors (such as isoprene, monoterpenes, and amines) play important roles in the formation and growth of new particles in the Arctic (Leaitch et al., 2013; Willis et al., 2016; Park et al., 2017; Abbatt et al., 2019; Mungall et al., 2016). In addition, iodine oxides significantly contribute to NPF in marine and coastal Arctic environments owing to emissions from marine microalgae at low tide or snowpack photochemistry in ice and snow-covered regions (Allan et al., 2015; O'Dowd et al., 2002; Raso et al., 2017). Biogenic gaseous precursors released by the melting Arctic sea-ice margins have also been associated with NPF (Dall´Osto et al., 2017; Willis et al., 2018). Recent studies in Alaska have indicated that the formation and growth of particles are influenced by emissions from oil and gas extraction activities in Prudhoe Bay (Gunsch et al., 2017; Kolesar et al., 2017). Although several observations have been made in the Arctic under different environmental conditions (Burkart et al., 2017b; Collins et al., 2017), there are few detailed size distribution analyses of particle formation and growth events within the Arctic marine environment.

Several studies have attempted to investigate the impacts of NPF on the concentrations of cloud condensation nuclei (CCN) (Willis et al., 2016; Burkart et al., 2017b; Collins et al., 2017). Model-based studies have predicted that a large fraction of CCN (up to 78% of CCN at 0.2 % supersaturation) in the global atmosphere results from atmospheric NPF and growth (Merikanto et al., 2009; Westervelt et al., 2014; Spracklen et al., 2008). Field observations have also observed substantial increases in the concentrations of CCN due to atmospheric nucleation in various environments (Pierce et al., 2012; Kalivitis et al., 2015; Burkart et al., 2017b; Collins et al., 2017; Kim et al., 2019). Several examples of increase in the CCN concentration after a few hours from the beginning of NPF events were presented by Burkart et al. (2017b) in the summer marine Arctic during the 2014 NETCARE Amundsen ice breaker campaign, by Kim et al (2019) at King Sejong Station in the Antarctic Peninsula, by Pierce et al. (2012) in a forested mountain valley in western Canada, and by Willis et al. (2016) in an Arctic aircraft campaign in Nunavut, Canada. However, due to the infrequency of aerosol measurements collected onboard ice breakers, very few studies have measured the simultaneous aerosol size distribution and

CCN concentrations over the Arctic Ocean.

In this study, the physical characteristics of aerosol particles over the Arctic and Pacific Oceans were investigated between August 31 and September 24, 2017, using aerosol particle monitoring instruments installed on the Korean ice breaker R/V Araon. Data of the aerosol size distribution, the concentrations of the total aerosol number (CN), black carbon (BC), and CCN were continuously collected using various aerosol instruments. The main aims of this study were to (1) investigate the frequency and characteristics of NPF and particle growth over the Arctic and Pacific Oceans, (2) determine the major sources that are associated with NPF based on backward air mass trajectory analysis, and (3) explore the potential contribution of NPF to the CCN concentrations in the remote marine environment.

2. Experimental methods

2.1. Study area and ship tracks

Ambient atmospheric aerosol measurements were collected over the Arctic and Pacific Oceans onboard the ice breaker R/V Araon, operated by the Korea Polar Research Institute (KOPRI), Korea. The ship's track is presented in Fig. 1. The cruises covered two main areas: the Arctic Ocean (including both Beaufort and Chukchi Seas) and the remote Northwest Pacific Ocean. The ship departed from Barrow, USA, on August 28, 2017, crossed the Beaufort (August 29-September 13, 2017) and Chukchi Seas (September 15, 2017), and reached Nome, USA, on September 16, 2017. The Beaufort Sea extends across the northern coasts of Alaska and the Northwest Territories of Canada. After completing the Arctic survey, the ship departed from Nome, USA, on September 18, 2017, crossed the Bering Sea, Sea of Okhotsk, and East Sea, and reached Busan, Korea, on September 28, 2017.

2.2. Atmospheric aerosol measurements

The aerosol sampling inlet was placed on the front deck of the ship (13 m above sea level), ahead of the ship's engines to avoid any influences from the emissions of the ship's exhaust. In addition, kitchen ventilation systems were connected by a plastic cylindrical pipe (~15 m length) and moved back on the

deck (far away from the sampling inlet) to minimize the potential effects of cooking emissions on the atmospheric measurements during the sampling periods. Aerosols were sampled through a stainless steel tube (inner diameter of 1/4 in, and length of ~1 m), which was connected to the various instruments by electrically conductive tubing to minimize particle losses in the sampling line.

The physical properties of the aerosols were measured with various aerosol instruments, including two condensation particle counters (TSI 3776 CPC and TSI 3772 CPC), two scanning mobility particle sizers (SMPS), an optical particle sizer (OPS), an aethalometer, and a cloud condensation nuclei counter (CCNC). The TSI 3776 CPC and TSI 3772 CPC measured the total number concentrations of particles larger than 2.5 and 10 nm every 1 sec, respectively. The aerosol sample flow rates of TSI 3776 CPC and TSI 3776 CPC were 1.5 and 1.0 lpm, respectively. The number size distributions of the particles were measured using the nano SMPS every 3 min (Differential mobility analyzer (DMA): TSI 3085, CPC: TSI 3776), covering a size range of 3 to 63.8 nm, and the standard SMPS (DMA: TSI 3081, CPC: TSI 3772) every 3 min, covering a size range of 10 to 300 nm. The aerosol and sheath flow rates of the nano-SMPS were 1.5 and 15 lpm, respectively; and those of the standard SMPS were 1.0 and 10 lpm, respectively. An OPS (TSI 3330) was used to determine the size distribution of particles in the range of 100 nm to 10 μm diameter with a sample flow rate of 1.0 lpm every 3 minutes. The BC concentration was measured using an aethalometer (AE22, Magee Scientific Co., USA) with a 5-min time resolution to assess the influence of anthropogenic sources (such as local pollution and ship emissions). The instrument uses the absorption of light at a wavelength of 880 nm by the ambient aerosols collected on a quartz filter tape to determine the BC concentration. The flow rate through a sharp-cut 2.5 μm cyclone (BGI, Inc., USA) was set to 5 lpm and the integration time was 5 min. The Droplet Measurement Technologies CCN counter (DMT CCN-100) was operated to measure the CCN number concentrations. The total flow rate in the CCN counter was 0.5 lpm, and the counter was operated at five different supersaturation ratios (SS) (0.2, 0.4, 0.6, 0.8, and 1.0 %) every 30 min. The sample and sheath flow rates of the CCN counter were 0.05 and 0.45 lpm, respectively.

2.3. Identification of ship exhaust

To obtain a data set that reflects background aerosol loading, measurement data affected by the exhaust emissions of the ship's engine should be excluded prior to further data analysis. For this, aerosol data were filtered based on the BC concentration, wind direction, wind speed, and total particle number concentration. The data with the following properties were discarded: (1) BC concentrations exceeding 100 ng m^{-3}, (2) relative wind direction against the ship's heading between 110° and 260°, as this originates directly from the ship's exhaust, (3) relative wind speed lower than 2 m sec^{-1} as air masses under a calm environment could become contaminated due to local turbulence, and (4) the total particle number concentrations were particularly high (spike) and varied dramatically in a short time. Ship plumes were clearly observed in the data collected during the campaign. The data collected when total aerosol number concentrations were higher than 8000 cm^{-3} were removed. In addition, the CPC and SMPS data were removed for the time periods when total aerosol number concentrations suddenly increased more than two times higher than the background values. Typically, the ship exhaust differs from the NPF events as the enhanced number concentration during the NPF events lasted for at least an hour with a low BC concentration (Ehn et al., 2010).

2.4. Backward air mass trajectory and satellite observations

The backward air mass trajectories were analyzed using version 4 of the Hybrid Single-Particle Lagrangian Integrated Trajectory (HYSPLIT) model (http://ready. arl.noaa.gov/) to examine their relationships with the physical characteristics of aerosol particles. The 2-day air mass back trajectories (48 h) were determined at hourly intervals from the ship's position at an arrival height of 50 m to estimate the transport history of the air masses arriving at the observation site (Park et al., 2018). The potential origins of the aerosols were divided into three categories based on the retention time of the 2-day back trajectories over the three major domains: Arctic Ocean (including the Beaufort and Chukchi Seas, and sea-ice region), Pacific Ocean (including the Bering Sea and Sea of Okhotsk) and land (including Alaska and the eastern part of Siberia) (Fig. 1). The phytoplankton biomass was obtained by

calculating the chlorophyll-*a* concentration from the level-3 product of Aqua Moderate Resolution Imaging Spectroradiometer at a 4 km resolution (Fig. S1). Geographical information over the ocean, land and sea-ice was obtained from the sea-ice index, which was provided by the National snow and Ice Data Center (NSIDC) (Fig. S2). Note that the sea-ice extent was defined as the area having an ice concentration of ≥ 15% (Pang et al., 2018). Air masses that intensively passed over the Beaufort and Chukchi Seas and sea-ice region were categorized as Arctic Ocean originated air masses (i.e., > 50% retention over the ocean > 65^{o}N and sea-ice region). Air masses that intensively passed over Northern Alaska and the eastern Siberia were potentially affected by the Arctic tundra and categorized as land originated air masses (i.e., > 50% retention over the land domain). Finally, air masses that traveled through the Bering Sea and Sea of Okhotsk were categorized as air masses originated from Pacific Ocean domain (i.e., > 50% retention over the ocean domain < 65^{o}N).

2.5. Oceanic measurements

To examine the influence of oceanic conditions on NPF and growth, seawater samples were collected from sea surface at a depth of ~ 1 m by Niskin bottles. The sampling locations and methods have been described previously in more detailed (Park et al., 2019). In brief, concentrations of dissolved organic carbon (DOC) were measured with a Shimadzu TOC-V high-temperature combustion total organic carbon analyzer. To identify the source and composition of DOC in surface seawater, three-dimensional excitation-emission matrixes (EEMs) were scanned using a fluorescence spectrometer (Varian, USA). The excitation wavelength range was between 250 and 500 nm, and emission between 280 and 600 nm. In this study, the four major fluorescent components were classified into 4 groups; terrestrial humic substances peak (A) (EX: 260 nm, EM: 380−460 nm), the terrestrial fulvic substances peak (C) (EX: 350 nm, EM: 420−480 nm), the marine fulvic substances peak (M) (EX: 312 nm, EM: 380−420 nm), and the proteinaceous peak (T) (EX: 275 nm, EM: 340 nm) (Coble, 2007).

3. Results and discussion

3.1. Overall particle number concentrations

Fig. 2a presents a time series of the 1 hour average total particle number concentration (CN) measured using TSI 3776 CPC and TSI 3772 CPC throughout the sampling periods. The number concentration of particles larger than 2.5 nm ($CN_{2.5}$) or 10 nm (CN_{10}) in the Arctic and Pacific marine environments had a range of approximately three orders of magnitude ($\sim 10^1 - 10^3$ cm^{-3}). In most cases, the $CN_{2.5}$ and CN_{10} concentrations were less than ~2000 cm^{-3}, with averages of 505 ± 280 and 492 ± 264 cm^{-3}, respectively, which were in agreement with those reported in previous studies conducted at other Arctic stations (Asmi et al., 2016; Burkart et al., 2017a; Freud et al., 2017) and remote marine regions (O'Dowd et al., 2014; Sellegri et al., 2006; Kim et al., 2019; Jang et al., 2019; Yum et al., 1998; Hudson and Yum, 2002). For example, four years of observational data from the Arctic Climate Observatory in Tiksi, Russia, showed that the monthly median CN concentration ranged from ~184 cm^{-3} in November to ~724 cm^{-3} in July (Asmi et al., 2016). Furthermore, Sellegri et al. (2006) reported CN concentrations under clean marine sector conditions at Mace Head of a few hundreds of cm^{-3} (e.g., ~200 cm^{-3} in January and ~450 cm^{-3} in June). Elevated $CN_{2.5}$ and CN_{10} concentrations were concentrated over the period from September 13 to 20, when the ship sailed over Chukchi and Bering Seas. During this period, $CN_{2.5}$ and CN_{10} concentrations exceeding ~2000 cm^{-3} were frequently observed. The peak concentrations of aerosol particles were notable, as the $CN_{2.5}$ and CN_{10} concentrations exceeded ~6016 and ~5750 cm^{-3}, respectively.

To elucidate further details of the variations in $CN_{2.5}$ and CN_{10}, the particle size distributions measured with the nano SMPS, standard SMPS, and OPS were divided into four size groups: nucleation (3 − 20 nm), Aitken (20 − 100 nm), accumulation (100 − 300 nm), and coarse (> 300 nm from OPS), as shown in Fig. 2b−e. The average number concentrations of the nucleation-mode (N_{NUC}), Aitken-mode (N_{AIT}), accumulation-mode (N_{ACC}), and coarse-mode (N_{OPS}) particles were 169 ± 142, 201 ± 131, 40 ± 17, and 4 ± 2 cm^{-3}, respectively. The temporal variations in N_{NUC} and N_{AIT} exhibited a distinct pattern, compared to that of N_{ACC} and N_{OPS}. Overall, N_{NUC} and N_{AIT} concentrations larger than ~1000 cm^{-3} were observed from September 13 to 20 (e.g. the ship sailed over Chukchi and Bering Seas), whereas

relatively high concentrations of N_{ACC} and N_{OPS} were observed from September 21 to 23 (e.g., the ship sailed over Sea of Okhotsk). As shown in Fig. 2b, sudden bursts of nucleation-mode particles occurred frequently, as indicated by a sudden increase in the N_{NUC} concentration rising from tens to several thousands of cm^{-3}. Whenever the $CN_{2.5}$ concentration exceeded ~2000 cm^{-3}, the N_{NUC} concentration exceeded ~600 cm^{-3} (except for the results observed in the evening of September 18). In addition, the $CN_{2.5}$ concentration was strongly correlated with the N_{NUC} concentration (r^2 = 0.69) (Fig. S3), suggesting that the high CN concentration was mainly derived from nucleation-mode particles. Instances of elevated N_{NUC} occurred along the northern coast of Alaska (September 13 – 14, 2017), throughout the Chukchi Sea (September 15, 2017), near the Nome and Eastern Siberia (September 16 – 18, 2017), and throughout the Bering Sea (September 19 – 20, 2017). During the cruises, the satellite-derived chlorophyll-*a* concentration data indicated strong biological activity over the Chukchi and Bering Seas, as shown in Fig. S1. Thus, the high occurrence of nucleation-mode particles may be related to multiple processes that influence the formation of secondary aerosols (e.g., oceanic biological activities, regional anthropogenic emissions on land (Alaska or eastern Siberia), and terrestrial sources in the tundra ecosystems of Alaska).

3.2. Case studies

As mentioned in Section 3.1, significant increases in N_{NUC} were frequently observed during the cruise (Fig. 2 b). Typically, N_{NUC} is used to indicate the presence of newly formed particles produced by gas-to-particle conversion (i.e., secondary aerosol formation) (Asmi et al., 2016; Burkart et al., 2017a). Here, an NPF event was defined as a sharp increase in the N_{NUC} with elevated $CN_{2.5}$ that lasted for at least one hour. Fig. 3 presents contour plots of the size distributions measured using nano SMPS and standard SMPS. This strong NPF and growth event occurred over the Chukchi and Bering Seas, which border the western and northern sides of Alaska, suggesting that there may be a substantial source of precursors in this region. Bursts of the smallest particles at the lowest detectable sizes (~2.5 nm) were not observed; however, we hypothesize that, during the NPF event, particle formation occurred

elsewhere and that subsequent horizontal extension caused the 1particles to reach the sampling site. Previously, NPF events have been identified on the regional scale in several locations around the world (Kerminen et al., 2018; Németh and Salma, 2014; Tremblay et al., 2019; Vana et al., 2004; Väänänen et al., 2013). For instances, Németh and Salma (2014) found that a nucleating air mass in regional NPF events may originate horizontally as far as several hundreds of kilometers (~400 or 700 km) away from the sampling site. Tremblay et al (2019) also concluded that particle nucleation events occurred over spatial scales of at least 500 km during the summertime in the Canadian High Arctic. In this section, case studies are discussed, including (i) marine Arctic NPF event, (ii) terrestrial Arctic NPF event, and (iii) pacific marine aerosol categories. During these temporal periods, the influences of the origins and pathways of air masses on the characteristics of particle formation and growth were investigated.

3.2.1. Open ocean marine Arctic NPF event case study

The marine Arctic NPF event was observed on September 3, 2017, and time series plots of the particle size distribution and air mass origins are presented in Fig. 4. N_{NUC} increased from 77 cm^{-3} to 757 cm^{-3}, while N_{AIT} varied little. The elevated number concentration of nucleation-mode particles lasted for over five hours and then disappeared. Geometric mean diameter (GMD) varied from 14.6 to 18.2 nm with an average of 16.3 nm, indicating that particle growth hardly occurred. The GMD is defined as the particle diameter at which the cumulative probability becomes 50% for the fitted log-normal distribution (Hinds, 1999). During the day, air masses traveled over the Arctic Ocean (explicitly, 47.6, 0 and 0.4 h over the Arctic Ocean, Pacific Ocean and land domain, respectively), and have been categorized as Arctic Ocean originated air masses. As shown in Fig. S1, the satellite-derived chlorophyll-*a* concentration indicated a relatively high level of biological activity in the ocean during the time period focused upon in this study. It was noteworthy that the monthly mean chlorophyll concentration in the Beaufort and Chukchi Seas (2.24 ± 3.44 mg m^{-3}; 65°N−74°N and 170°E−120°W) was approximately 3-fold greater than that estimated in the Pacific Ocean including the Bering Sea and the Sea of Okhotsk (0.83 ± 1.30 mg m^{-3}; 40°N−65°N and 145°E−168°W) (Fig. S1). Moreover, the

marginal ice zone is commonly associated with intense algae blooms during the melting season, therefore, significant emissions of biogenic trace gases such as DMS have been detected in the sea-ice edge (Levasseur, 2013; Oziel et al., 2017). Accordingly, as our measurements were collected over the Arctic Ocean onboard the ice breaker, marine biogenic sources could be considered as an important factor inducing NPF events.

Fig. 4d shows cosine of the solar zenith angle (cos (SZA)) data that can be used as a proxy for solar energy reaching the ground surface. In addition, cloudiness which usually affects the real solar radiation reaching the surface was compared based on Moderate Resolution Imaging Spectroradiometer (MODIS) cloud fraction retrievals (Fig. S5). The data showed that cloud fraction was significantly high during the entire sampling periods, in general agreement with some other studies over the western Arctic region (e.g., Dong et al., 2010; Collines et al., 2017). In detail, the cloud fraction was relatively low for week 1 (8/29/2017− 9/5/2017; Fig. S5a) and week 3 (9/14/2017− 9/21/2017; Fig. S5c) when NPF event and growth was frequently observed (Fig. 3). This suggests that solar radiation at the surface, which is affected both by the cloud cover and SZA, may have influenced aerosol concentration and NPF observed here. As illustrated in Fig 4, the NPF event occurred when the sun was below the horizon (i.e., Arctic nighttime nucleation). Typically, nucleation tends to take place preferably with high solar irradiation during the daytime (Kulmala et al., 2004). In several locations, however, also nighttime nucleation has been observed at Tumbarumba in Australian (Suni et al., 2008), at Värriö measurement station in Finnish Lapland (Vehkamäki et al., 2004), and at a subarctic site in northern Sweden (~14 km east of Abisko) (Svenningsson et al., 2008). The possible explanation for nighttime events is that the actual formation and growth occurred even during daylight, but very slow growth in the Arctic and marine atmosphere allowed to detect the particles (~ 8 nm) only after sunset (Vehkamäki et al., 2004). Previous study reported that 32% of strong nighttime nucleation events (2.5 times as frequent as daytime nucleation event) were appeared in the presence of a very efficient ion source such as the strong radon efflux from the Tumbarumba soil (Suni et al., 2008). Due to their rarity, the major mechanisms for nocturnal aerosol production are still unclear and require more study.

3.2.2. Open ocean terrestrial Arctic NPF event case study

The terrestrial Arctic NPF event was observed during September 13−14 2017. As shown in Fig. 5, significant strong NPF events occurred frequently during this period. The number concentration of total particles increased considerably, as a $CN_{2.5}$ value exceeding ~6016 cm^{-3} was observed during this event. In addition, the average concentrations of N_{NUC} and N_{AIT} during the terrestrial Arctic NPF were 931 ± 222 and 1127 ± 380 cm^{-3}, respectively. This indicates that high $CN_{2.5}$ concentration mainly contributed by nucleation and Aitken-mode particles (45 and 54% of the size distribution for nucleation-mode and Aitken-mode particles, respectively). GMD increased from 13.9 to 33.3 nm, indicating that the nucleation-mode particles subsequently increased in size. The formation and growth of aerosol particles were observed during the daytime (Fig. 5d), suggesting that photochemistry is involved. During this period, air masses were heavily influenced by northern Alaska. The average retention times of the 2-day back trajectories arriving at the ship position over the northern Alaska, Arctic Ocean and Pacific Ocean were 40.8, 7.2 and 0 h, respectively (Fig. 5e). It can be seen that the photochemical reactions of precursor gases (e.g., volatile organic compounds (VOCs) such as isoprene, monoterpenes, and sesquiterpenes) emitted by terrestrial ecosystems in Alaska were associated with new particle formation and growth (Schollert et al., 2014; TAPE et al., 2006; Kolesar et al., 2017; Ström et al., 2003).

3.2.3. Pacific marine aerosol case study

A typical aerosol scenario for Pacific marine air masses was observed on September 21−22, 2017, when the air masses passed over mainly the Pacific Ocean (including the Bering Sea and Sea of Okhotsk) (explicitly, 0, 47.9 and 0.1 h over the Arctic Ocean, Pacific Ocean and land domain, respectively) (Fig. 1a). As shown in Fig. 6, the aerosol number concentrations exhibited a bimodal size distribution, peaking at size ranges of 30 – 80 nm (Aitken mode) and 100 – 300 nm (accumulation mode), respectively. In contrast, the concentrations of nucleation-mode particles were very low. For example, the concentration of N_{NUC} ranged from 1 to 38 cm^{-3} with an average of 8 ± 4 cm^{-3}. We also

observed $CN_{2.5}$ values at the background level of ~460 ± 70 cm^{-3}, which are consistent with the measurements collected at a coastal Antarctic station during summer (~600 cm^{-3}) (Kim et al., 2017) and from flight-based measurements over the Arctic Ocean (~300 cm^{-3}) (Burkart et al., 2017a).

3.3. Overview of aerosol properties according to different air mass back trajectories

Air masses comprising marine Pacific along with marine and terrestrial Arctic air masses were encountered during the campaign. In the section 3.2, two case studies of NPF events (Fig. 4 and Fig. 5) were found in the Arctic atmosphere. As stressed in Willis et al., (2018), NPF and growth is frequently observed in the boundary layer in the both Arctic open ocean and coastal regions. These events seem to occur more frequently than lower-latitude marine boundary layers (Quinn and Bates, 2011); there are multiple reasons including summer 24-h high solar radiation, low condensation sink, low temperature and low mixing of surface emissions, as recently reviewed in Abbatt et al. (2019). Our study also confirmed that any NPF was not detected during the Pacific transect.

In this section, we present an overall meteorological air mass summary of the open ocean field study, categorizing it into three synoptic period types: Pacific marine, Arctic marine and Arctic terrestrial. These classifications do not represent specific air mass back trajectories analysis, but they can mainly represent air masses that have been travelled over these three distinct geographical regions (section 2.4). Average size distributions for the three selected periods in the different air masses are shown in Fig. 7. To obtain the number size distribution in the size range from 7 nm to 300 nm as shown in Fig. 7, we used nano SMPS data from 7 nm to 64 nm and standard SMPS data from 64 nm to 300 nm. The nano SMPS and standard SMPS data agreed within ~8.8% in their overlapping size range (10 – 64 nm) (Fig. S4), similar to a previous study (Watson et al., 2011). In addition, a summary of total number concentrations of particles for these periods is included in Table 1.

- *Arctic Marine*. A trimodal distribution was seen at 18 ± 3 nm, 53 ± 6 nm and 150 ± 6 nm. The first mode is due to NPF arriving from open pack sea ice and open ocean Arctic regions, as discussed in

Section 3.2.1 where a case study is presented. The Aitken mode (~53 nm) is remarkably similar to the Pacific Ocean aerosol size distribution and to previous studies detected in the Arctic regions (Tunved et al., 2013; Freud et al., 2017; Dall'Osto et al., 2019). The largest mode at ~150 nm may be due to a combination of primary and secondary aerosol components.

- *Arctic terrestrial*. A bimodal distribution is seen with two main modes at 24 ± 3 nm and 151 ± 3 nm, respectively. The nucleation and Aitken modes are much higher than the accumulation mode, suggesting that NPF governs the aerosol processes in this coastal region at this time of the year.

- *Pacific marine*. The Pacific Ocean aerosol size distributions showed a trimodal size distribution at 56 ± 3 nm, 130 ± 3 nm and 220 ± 6 nm. The lowest peak at ~56 nm (i.e., Aitken mode) is likely a combination of primary and secondary marine aerosol components, whereas the largest peak at ~220 nm might be caused by cloud processing and aged aerosols. The mode at ~130 nm could originate from primary sea spray aerosols in the Pacific atmosphere (Quinn et al., 2015). When the distribution is fitted with log-normal modes, the inter-modal minimum is calculated to be ~120 nm - often known as Hoppel minimum as a signature of cloud processing (Hoppel et al., 1994) - although, it is difficult to draw a firm conclusion due to the overlap with the third mode at ~130 nm.

This study shows that aerosol originating from higher and lower marine latitudes – although both being treated as marine air masses - have very different features, as pointed out in several previous studies (Dall'Osto et al., 2010; Frossard et al., 2014). A key conclusion of this study is that we also need to separate different bioregions in the Arctic, especially given the current results showing very different aerosol size distributions in the Arctic study areas (Fig. 7; Arctic marine and Arctic terrestrial). The reasons for the much higher aerosol concentrations near the coast of Alaska relative to the open ocean sympagic and pelagic regions may be multiple. We discuss at least two major sources may contribute to the high aerosol concentrations recorded.

The first source of aerosols in the late summer terrestrial Arctic air masses may be due to

anthropogenic sources. Due to sea ice retreat and better technologies, the Arctic is now easily accessible to human activities, including oil and gas extraction (Law and Stohl, 2007; Peters et al., 2011). These Arctic oil fields can emit the large amounts of aerosols, and with on-going Arctic development, such local combustion emissions may increase in the future, possibly affecting local air quality (Gunsch et al., 2017; Schmale et al., 2018a). In fact, some NPF events were reported within the North Slope of Alaska (e.g., Prudhoe Bay oil fields) during August and September 2016 at Oliktok Point Alaska. This observation was suggested to be linked with oil fields emissions (Kolesar et al., 2017). However, our measurements were conducted in the open ocean, quite far from any land oil field local emissions. BC data were collected as shown in Fig. 8; they revealed very high standard deviations due to high detection limit of the instrument used relative to the concentrations detected. However, no remarkable differences can be seen, all pointing to pristine clean marine air masses with BC values of approximately 20 ± 10 ng m^{-3}. The two Arctic categories (Marine and Terrestrial) shows similar BC values, whereas higher values can be seen for the Pacific marine aerosol category, probably due to contamination from nearby Asian high pollutant sources.

The second source of aerosol in the late summer terrestrial Arctic air masses may be due to terrestrial natural sources. We believe that this may be a much more probable reason. The Arctic Ocean is submerged under areas of relatively shallow water known as a shelf sea for ~50% of its area. It is a relatively small ocean, characterized by pronounced riverine influence and a complex hydrography. Up to 11% of the entire global river discharge ends up in the Arctic Ocean (Shiklomanov et al., 2000), which is only 1% of the global ocean volume. The discharge of freshwater is increasing (Peterson et al., 2002), impacting coastal salinity and carbon cycle. Indeed, this continental runoff is a major source of freshwater, nutrients and terrigenous material to the Arctic Ocean (Benner et al., 2005; Fichot et al., 2013; Massicotte et al., 2017). The warming climate in the region is causing permafrost degradation, alterations to regional hydrology and shifting amounts and composition of dissolved organic matter (DOM) transported by streams and rivers (Mann et al., 2016; Chen et al., 2017). Overall, there is a considerable spatial and temporal heterogeneity in the distribution of the DOC in the Arctic, owing to

strong biological and physicochemical processes. It is important to remember that sea ice formation and melting also affects the concentrations and distributions of DOC, although its impact is still difficult to resolve (Fichot et al., 2013; Shen et al., 2012).

In a recent paper (Park et al., 2019), we suggested that the large amount of freshwater from river runoff may have a substantial impact on primary aerosol production mechanisms, possibly affecting the cloud radiative forcing. We showed that the Artic riverine organic matter can be directly emitted from surface seawater into the atmosphere via bubble bursting (Park et al., 2019). The high amount of DOC populating the sea-surface microlayer (SML) in the Arctic waters - including UV absorbing humic substances - can also produce VOCs (Ciuraru et al., 2015; Fu et al., 2015), which are known precursors of secondary organic aerosols. Recently, Mungall et al. (2017) reported that the marine microlayer in the Canadian Arctic Archipelago is a source of oxidized VOCs (OVOCs), which could be an important source of biogenic secondary organic aerosol (Croft et al., 2019). Previous studies also reported fluorescent water-soluble organic aerosols in the High Arctic atmosphere (Fu et al., 2015). It is worth noting that terrestrial VOCs from tundra and lakes at elevated concentrations were reported (Potosnak et al., 2013; Lindwall et al., 2016; Steinke et al., 2018).

Fig. 9 shows DOC concentrations from water samples taken in the areas where the NPF marine and terrestrial case studies (Section 3.2.1 and 3.2.2) were detected. It is clear that as much as twice higher concentrations are seen for the coastal marine areas, relative to the open ocean marine regions. The origin of this organic matter can be obtained by the FDOM analysis. Fig. 9 (bottom) shows specific peaks attributed to different chemical features. The ratio of terrestrial humic substances (peak A) was 3.5 for the terrestrial/marine samples. By striking contrast, marine fulvic substances (peak M) and proteinaceous (peak T) had a ratio of 0.45 and 0.27, respectively, showing two very distinct chemical compounds. This suggests that coastal oceanic water enriched in river organic material as well as fresh water tundra and lake may be a source of VOC (both from biotic and abiotic emission processes) that may be responsible for the high secondary aerosols detected near these areas.

3.4. Particle growth rates and condensation sink

Table 1 shows particle growth rate (GR) and condensation sink (CS) for Arctic marine, Arctic terrestrial and Pacific marine air masses. The GR was calculated by fitting a linear regression to the peak diameter of the aerosol size distribution for the nucleation-mode between 4 and 20 nm against time during the NPF cases (Dal Maso et al., 2005; Pierce et al., 2014). The GR observed during the Arctic marine and Arctic terrestrial air masses were the 0.4 ± 0.3 nm h^{-1} and 0.8 ± 0.2 nm h^{-1}, respectively, which was similar to the values previously observed from other Arctic regions. A shipboard expedition conducted during the summers of 2014 and 2016 throughout the Canadian Arctic, indicated that the GR varied widely from 0.2 to 15.3 nm h^{-1} (Collins et al., 2017). The GR observed at Summit, Greenland was 0.2 ± 0.1 nm h^{-1} (range of 0.09 to 0.3 nm h^{-1}) (Ziemba et al., 2010). Similarly, in Utqiagivik (Barrow), Alaska, the GR was 1.0 nm h^{-1} in air mass influenced by Beaufort Sea, whereas the value was 11.1 nm h^{-1} in air mass influenced by Prudhoe Bay (i.e., oil field area) (Kolesar et al., 2017). Particularly, simultaneous growth of multiple modes was present in some cases (9/13/2017− 9/21/2017). We calculated the GR of the distinct modes, as shown in Fig. S6. The results showed that growth of the larger mode (e.g., preexisting mode) was faster than the smaller mode (e.g., nucleation mode), consistent with ship-based aerosol measurements in the summertime Arctic by Burkart et al. (2017b). They proposed that growth was largely via condensation of semi-volatile organic material, because lower volatile organics could lead to faster growth of the smaller mode.

The CS is a key parameter assessing the NPF and growth and determines how rapidly gaseous molecules condense onto pre-existing particles. The CS was calculated, following Dal Maso et al. (2002) and Collines et al. (2017). The resulting CS values are given in Table 1. The CS observed during the Arctic marine and Arctic terrestrial air masses were 0.5 ± 0.4 nm h^{-1} and 0.9 ± 0.5 nm h^{-1}, respectively. The CS in this study is on the low end of the values observed during the summer in Arctic marine boundary layer (shipborne expeditions) (Collins et al., 2017), Utqiagivik, Alaska (Kolesar et al., 2017), and Ny-Ålesund, Svalbard (Giamarelou et al., 2016). In case when air mass passed over the Pacific Ocean, the CS was 2 or 4 times higher than those of Arctic air masses. It seems that such higher

CS for Pacific marine air masses lowered the concentration of condensable vapors, thereby resulting in the non-event days in Pacific marine air masses.

3.5. Impact on CCN number concentrations

Fig. 10a illustrates the CCN concentrations for the three selected periods under different supersaturation conditions. For a given SS of 0.4%, CCN concentrations for Arctic marine, Arctic terrestrial and Pacific marine air masses were 35 ± 40 cm^{-3}, 71 ± 47 cm^{-3}, and 204 ± 87 cm^{-3}, respectively. Higher concentrations of CCN were observed when the air mass originated from the Pacific marine for a SS of 0.2%–1.0 %. This may have occurred due to the differences in the CCN sources between the Arctic and Pacific Oceans. It was noted that that accumulation and coarse-mode particles, which are predominant over the Pacific Ocean (Fig. 7), can easily act as CCN. Our results agreed well with values reported in previous studies that measured CCN at a ground-based Arctic station (Jung et al., 2018), but was slightly higher than those measured from high-Arctic expeditions (Leck et al., 2002; Martin et al., 2011; Mauritsen et al., 2011). For example, Jung et al. (2018) reported seasonal variations in the CCN concentration over seven years (2007 –2013) at the Zeppelin station, and found that the monthly mean CCN concentrations ranged from 17 cm^{-3} in October 2007 to 198 cm^{-3} in March 2008 at a SS value of 0.4%. However, Mauritsen et al. (2011) observed CCN concentrations lower than ~100 cm^{-3} at five different supersaturations (SS = 0.10%, 0.15%, 0.20%, 0.41%, and 0.73%), with median values ranging from 15 to 50 cm^{-3}, in four High Arctic expeditions during the Arctic Summer Cloud Ocean Study. Such values were also in line with the long term measurement at an Arctic station in Barrow, which indicated that the median CCN concentrations at 0.2% SS was smaller than 100 cm^{-3} (Schmale et al., 2018b).

We also compared CCN activity and critical diameter for the three selected periods, as shown in Fig. 10b and c. The CCN activity is defined as the ratio of the number concentration of particles that activated to become CCN at a given supersaturation to the total number concentration of particles larger than 2.5nm ($CN_{2.5}$). The CCN activity followed a similar pattern as the CCN concentration. Furthermore, the critical diameter (D_c) (i.e., the diameter at which the integration of aerosol size

distribution from the largest particle diameter to the lower ones matches with the measured CCN concentration) was estimated using the measured aerosol size distribution, $CN_{2.5}$, and CCN concentrations with a time resolution of 1 h, as described by Furutani et al., (2014). The D_c at a SS of 0.4% was found to be 103 ± 43 nm, 83 ± 18 nm, and 136 ± 67 nm for Arctic marine, Arctic terrestrial, and Pacific marine periods, respectively. These values are comparable to previous studies obtained in the Arctic and subarctic regions. For instance, the D_c of 80 nm at 0.6 % SS was observed during the aircraft measurement in July 2014 in the high Arctic marine boundary layer of Resolute Bay, Nunavut, Canada (Burkart et al., 2017a). Jaatinen et al. (2014) reported that the D_c value of 98 ± 16 nm (SS = 0.4%) from the subarctic area of Finland (Pallas-Sodankylä Global Atmospheric Watch station). Anttile et al. (2012) also showed that a D_c value was in the range of 90 to 120 nm at a SS of 0.4% during the same filed campaign as reported in Jaatinen et al. (2014). For a maximum SS between 0.18 and 0.26%, D_c varied between 110 and 140 nm at the same measurement sites.

4. Summary and conclusions

This study presents the physical properties of aerosol particles measured aboard the R/V Araon ice-breaker during 2017 throughout the Arctic and Pacific Oceans. The $CN_{2.5}$ value commonly ranged between 13 and 2000 cm^{-3} with an average of 505 ± 280 cm^{-3}. An elevated $CN_{2.5}$ concentration reaching ~6016 cm^{-3} was observed from 13 September to 20 September. The temporal variations in the $CN_{2.5}$ concentration followed a similar pattern to those of N_{NUA} and N_{AIT}. We also found that the $CN_{2.5}$ concentration was strongly correlated with N_{NUA} (r^2 = 0.69), suggesting that CN was mainly derived from nucleation-mode particles.

NPF events caused by gas-to-particle conversion frequently occurred over the Arctic Ocean. Overall, two major NPF sources (i.e., Arctic marine and Arctic terrestrial) were identified based on the backward air mass trajectory analysis. NPF events were associated with Arctic marine air masses, indicating the impact of marine biogenic emissions from the Arctic Ocean. Strong NPF events with particle growth were associated with Arctic terrestrial air masses, which may be due to the biogenic

precursor gases emitted by terrestrial ecosystems including river discharge and Alaskan tundra in the Arctic coastal areas. In contrast, relatively larger particles with broad Aitken and accumulation-mode peaks were observed over the Pacific Ocean. Our study confirmed that any NPF was not detected during the Pacific transect. We also compared the average CCN concentrations for each of the cases. Our data showed that the impact of aerosols on CCN concentrations (SS = 0.4%) was significant: 35 ± 40 cm^{-3}, 71 ± 47 cm^{-3}, and 204 ± 87 cm^{-3} for Arctic marine, Arctic terrestrial, and Pacific marine periods, respectively. Our interpreted data showed that river outflows and tundra strongly influence Arctic aerosol properties. Further detailed measurements of the chemical characteristics of marine aerosols are required to provide more direct evidence for the contribution of biogenic precursors to the NPF and CCN in the remote Arctic atmosphere.

Arctic areas are currently experiencing drastic climate change, with air temperatures increasing at twice the rate of the global average. This warming is causing clear changes, such as the increases in biogenic emissions from tundra vegetation and changes in vegetation cover (Faubert et al., 2010; Peñuelas and Staudt, 2010; Potosnak et al., 2013; Lindwall et al., 2016). Lindwall et al. (2016) observed a 280% increase in VOC emissions relative to the ambient level in response to a 4 °C increase in the summer temperature of the Subarctic. Increases in VOC emissions from river discharge and tundra vegetation in the Arctic are critical factors that induce NPF and particle growth events, which may impact the CCN concentrations during the Arctic summer.

Data availability

The data analyzed in this publication are available from the Korea Polar Data Center (KPDC) (‘https://kpdc.kopri.re.kr/search/’), and also the raw data will be readily provided upon request to the corresponding author (yjyoon@kopri.re.kr).

Author contributions

JP, YJY designed the study, JP, MD’O, KP, YG, HJK, EJ, KTP, MP, SSY, JJ, and BYL analyzed data. JP, MD’O, KTP and YJY prepared the manuscript with contributions from all co-authors.

Competing interests

The authors declare that they have no conflict of interest.

Acknowledgements

We are grateful to the captain and crews of R/V *Araon* for their enthusiastic assistance during the cruise of ARA08C. This work was supported by a Korea Grant from the Korean Government (MSIP) (NRF-2016M1A5A1901769) (KOPRI-PN20081) and the KOPRI projects (PE17390 and PE20060). Kihong Park was supported by the National Leading Research Laboratory program (NRF-2019R1A2C3007202). Minsu Park and Seong Soo Yum were supported by National Research Foundation of Korea (NRF) grant (NRF-20180R1A2B2006965). Jinyoung Jung was supported by "Korea-Arctic Ocean Observing System (K-AOOS)", KOPRI, 20160245, funded by the MOF, Korea.

References

Abbatt, J. P. D., Leaitch, W. R., Aliabadi, A. A., Bertram, A. K., Blanchet, J. P., Boivin-Rioux, A., Bozem, H., Burkart, J., Chang, R. Y. W., Charette, J., Chaubey, J. P., Christensen, R. J., Cirisan, A., Collins, D. B., Croft, B., Dionne, J., Evans, G. J., Fletcher, C. G., Galí, M., Ghahremaninezhad, R., Girard, E., Gong, W., Gosselin, M., Gourdal, M., Hanna, S. J., Hayashida, H., Herber, A. B., Hesaraki, S., Hoor, P., Huang, L., Hussherr, R., Irish, V. E., Keita, S. A., Kodros, J. K., Köllner, F., Kolonjari, F., Kunkel, D., Ladino, L. A., Law, K., Levasseur, M., Libois, Q., Liggio, J., Lizotte, M., Macdonald, K. M., Mahmood, R., Martin, R. V., Mason, R. H., Miller, L. A., Moravek, A., Mortenson, E., Mungall, E. L., Murphy, J. G., Namazi, M., Norman, A. L., O'Neill, N. T., Pierce, J. R., Russell, L. M., Schneider, J., Schulz, H., Sharma, S., Si, M., Staebler, R. M., Steiner, N. S., Thomas, J. L., von Salzen, K., Wentzell, J. J. B., Willis, M. D., Wentworth, G. R., Xu, J. W., and Yakobi-Hancock, J. D.: Overview paper: New insights into aerosol and climate in the Arctic, Atmos. Chem. Phys., 19, 2527-2560, 10.5194/acp-19-2527-2019, 2019.

ACIA: Arctic Climate Impact Assessment, chap. 2, p. 23, Cambridge University Press, New York, USA,, 2005.

Allan, J. D., Williams, P. I., Najera, J., Whitehead, J. D., Flynn, M. J., Taylor, J. W., Liu, D., Darbyshire, E., Carpenter, L. J., Chance, R., Andrews, S. J., Hackenberg, S. C., and McFiggans, G.: Iodine observed in new particle formation events in the Arctic atmosphere during ACCACIA, Atmos. Chem. Phys., 15, 5599-5609, 10.5194/acp-15-5599-2015, 2015.

Asmi, E., Kondratyev, V., Brus, D., Laurila, T., Lihavainen, H., Backman, J., Vakkari, V., Aurela, M., Hatakka, J., Viisanen, Y., Uttal, T., Ivakhov, V., and Makshtas, A.: Aerosol size distribution seasonal characteristics measured in Tiksi, Russian Arctic, Atmos. Chem. Phys., 16, 1271-1287, 10.5194/acp-16-1271-2016, 2016.

Benner, R., Louchouarn, P., and Amon, R. M. W.: Terrigenous dissolved organic matter in the Arctic Ocean and its transport to surface and deep waters of the North Atlantic, Global Biogeochemical Cycles, 19, doi:10.1029/2004GB002398, 2005.

Burkart, J., Willis, M. D., Bozem, H., Thomas, J. L., Law, K., Hoor, P., Aliabadi, A. A., Köllner, F., Schneider, J., Herber, A., Abbatt, J. P. D., and Leaitch, W. R.: Summertime observations of elevated levels of ultrafine particles in the high Arctic marine boundary layer, Atmos. Chem.

Phys., 17, 5515-5535, 10.5194/acp-17-5515-2017, 2017a.
Burkart, J., Hodshire, A. L., Mungall, E. L., Pierce, J. R., Collins, D. B., Ladino, L. A., Lee, A. K. Y., Irish, V., Wentzell, J. J. B., Liggio, J., Papakyriakou, T., Murphy, J., Abbatt, J.: Organic condensation and particle growth to CCN sizes in the summertimemarine Arctic is driven by materials more semivolatile than at continental sites, Geophys. Res. Lett. 44, 10725–10734. https://doi.org/10.1002/2017GL075671, 2017 b.
Chang, R. Y.-W., Sjostedt, S. J., Pierce, J. R., Papakyriakou, T. N., Scarratt, M. G., Michaud, S., Levasseur, M., Leaitch, W. R., and Abbatt, J. P. D.: Relating atmospheric and oceanic DMS levels to particle nucleation events in the Canadian Arctic, Journal of Geophysical Research: Atmospheres, 116, doi:10.1029/2011JD015926, 2011.
Chen, X., Zhang, X., Church, J. A., Watson, C. S., King, M. A., Monselesan, D., Legresy, B., and Harig, C.: The increasing rate of global mean sea-level rise during 1993–2014, Nature Climate Change, 7, 492, 10.1038/nclimate3325 https://www.nature.com/articles/nclimate3325#supplementary-information, 2017.
Ciuraru, R., Fine, L., van Pinxteren, M., D'Anna, B., Herrmann, H., and George, C.: Photosensitized production of functionalized and unsaturated organic compounds at the air-sea interface, Scientific Reports, 5, 12741, 10.1038/srep12741 https://www.nature.com/articles/srep12741 #supplementary-information, 2015.
Coble, P. G.: Marine Optical Biogeochemistry: The Chemistry of Ocean Color, Chemical Reviews, 107, 402-418, 10.1021/cr050350+, 2007.
Collins, D. B., Burkart, J., Chang, R. Y.-W., Lizotte, M., Boivin-Rioux, A., Blais, M., Mungall, E. L., Boyer, M., Irish, V. E., Massé, G., Kunkel, D., Tremblay, J.-É., Papakyriakou, T., Bertram, A. K., Bozem, H., Gosselin, M., Levasseur, M., and Abbatt, J. P. D.: Frequent ultrafine particle formation and growth in Canadian Arctic marine and coastal environments, Atmos. Chem. Phys., 17, 13119–13138, https://doi.org/10.5194/acp-17-13119-2017, 2017.
Croft, B., Martin, R. V., Leaitch, W. R., Tunved, P., Breider, T. J., D'Andrea, S. D., and Pierce, J. R.: Processes controlling the annual cycle of Arctic aerosol number and size distributions, Atmos. Chem. Phys., 16, 3665-3682, 10.5194/acp-16-3665-2016, 2016.
Croft, B., Martin, R. V., Leaitch, W. R., Burkart, J., Chang, R. Y. W., Collins, D. B., Hayes, P. L., Hodshire, A. L., Huang, L., Kodros, J. K., Moravek, A., Mungall, E. L., Murphy, J. G., Sharma, S., Tremblay, S., Wentworth, G. R., Willis, M. D., Abbatt, J. P. D., and Pierce, J. R.: Arctic marine secondary organic aerosol contributes significantly to summertime particle size distributions in the Canadian Arctic Archipelago, Atmos. Chem. Phys., 19, 2787-2812, 10.5194/acp-19-2787-2019, 2019.
Dall'Osto, M., Ceburnis, D., Martucci, G., Bialek, J., Dupuy, R., Jennings, S. G., Berresheim, H., Wenger, J., Healy, R., Facchini, M. C., Rinaldi, M., Giulianelli, L., Finessi, E., Worsnop, D., Ehn, M., Mikkilä, J., Kulmala, M., and O'Dowd, C. D.: Aerosol properties associated with air masses arriving into the North East Atlantic during the 2008 Mace Head EUCAARI intensive observing period: an overview, Atmos. Chem. Phys., 10, 8413-8435, 10.5194/acp-10-8413-2010, 2010.
Dall'Osto, M., Beddows, D. C. S., Tunved, P., Harrison, R. M., Lupi, A., Vitale, V., Becagli, S., Traversi, R., Park, K. T., Yoon, Y. J., Massling, A., Skov, H., Lange, R., Strom, J., and Krejci, R.: Simultaneous measurements of aerosol size distributions at three sites in the European high Arctic, Atmos. Chem. Phys., 19, 7377-7395, 10.5194/acp-19-7377-2019, 2019.
Dall´Osto, M., Beddows, D. C. S., Tunved, P., Krejci, R., Ström, J., Hansson, H. C., Yoon, Y. J., Park, K.-T., Becagli, S., Udisti, R., Onasch, T., O´Dowd, C. D., Simó, R., and Harrison, R. M.: Arctic sea ice melt leads to atmospheric new particle formation, Scientific Reports, 7, 3318, 10.1038/s41598-017-03328-1, 2017.
Dal Maso, M.: Condensation and coagulation sinks and formation of nucleation mode particles in coastal and boreal forest boundary layers, J. Geophys. Res., 107, 10.1029/2001jd001053, 2002.
Dal Maso, M., Kulmala, M., Riipinen, I., Wagner, R., Hussein, T., Aalto, P. P., and Lehtinen, K. E. J.: Formation and growth of fresh atmospheric aerosols: Eight years of aerosol size distribution data

from SMEAR II, Hyytiälä, Finland, Boreal Environment Research, 10, 323-336, 2005.
Dong, X., Xi, B., Crosby, K., Long, C. N., Stone, R. S., and Shupe, M.: A 10 year climatology of Arctic cloud fraction and radiative forcing at Barrow, Alaska, J Geophys Res-Atmos, 115, D17212, doi.org/10.1029/2009JD013489, 2010.
Ehn, M., Vuollekoski, H., Petäjä, T., Kerminen, V.-M., Vana, M., Aalto, P., de Leeuw, G., Ceburnis, D., Dupuy, R., O'Dowd, C. D., and Kulmala, M.: Growth rates during coastal and marine new particle formation in western Ireland, J Geophys Res-Atmos, 115, doi:10.1029/ 2010JD014292, 2010.
Faubert, P., Tiiva, P., Rinnan, Å., Michelsen, A., Holopainen, J. K., and Rinnan, R.: Doubled volatile organic compound emissions from subarctic tundra under simulated climate warming, 187, 199-208, 10.1111/j.1469-8137.2010.03270.x, 2010.
Fichot, C. G., Kaiser, K., Hooker, S. B., Amon, R. M. W., Babin, M., Bélanger, S., Walker, S. A., and Benner, R.: Pan-Arctic distributions of continental runoff in the Arctic Ocean, Scientific Reports, 3, 1053, 10.1038/srep01053 https://www.nature.com/articles/srep01053#supplementary-information, 2013.
Freud, E., Krejci, R., Tunved, P., Leaitch, R., Nguyen, Q. T., Massling, A., Skov, H., and Barrie, L.: Pan-Arctic aerosol number size distributions: seasonality and transport patterns, Atmos. Chem. Phys., 17, 8101-8128, 10.5194/acp-17-8101-2017, 2017.
Frossard, A. A., Russell, L. M., Burrows, S. M., Elliott, S. M., Bates, T. S., and Quinn, P. K.: Sources and composition of submicron organic mass in marine aerosol particles, 119, 12,977-913,003, 10.1002/2014jd021913, 2014.
Fu, P., Kawamura, K., Chen, J., Qin, M., Ren, L., Sun, Y., Wang, Z., Barrie, L. A., Tachibana, E., Ding, A., and Yamashita, Y.: Fluorescent water-soluble organic aerosols in the High Arctic atmosphere, Scientific Reports, 5, 9845, 10.1038/srep09845, 2015.
Giamarelou, M., Eleftheriadis, K., Nyeki, S., Tunved, P., Torseth, K., and Biskos, G.: Indirect evidence of the composition of nucleation mode atmospheric particles in the high Arctic, J. Geophys. Res.-Atmos., 121, 965–975, https://doi.org/10.1002/2015JD023646, 2016.
Gunsch, M. J., Kirpes, R. M., Kolesar, K. R., Barrett, T. E., China, S., Sheesley, R. J., Laskin, A., Wiedensohler, A., Tuch, T., and Pratt, K. A.: Contributions of transported Prudhoe Bay oil field emissions to the aerosol population in Utqiaġvik, Alaska, Atmos. Chem. Phys., 17, 10879-10892, 10.5194/acp-17-10879-2017, 2017.
Hinds, W. C.: Aerosol Technology: Properties, Behavior, and Measurement of Airborne Particles, 2nd edn., Wiley-Interscience, New York, 1999.
Heintzenberg, J., Leck, C., and Tunved, P.: Potential source regions and processes of aerosol in the summer Arctic, Atmos. Chem. Phys., 15, 6487-6502, 10.5194/acp-15-6487-2015, 2015.
Heintzenberg, J., Tunved, P., Galí, M., and Leck, C.: New particle formation in the Svalbard region 2006–2015, Atmos. Chem. Phys., 17, 6153-6175, 10.5194/acp-17-6153-2017, 2017.
Hoppel, W. A., Frick, G. M., Fitzgerald, J. W., and Larson, R. E.: Marine boundary layer measurements of new particle formation and the effects nonprecipitating clouds have on aerosol size distribution, 99, 14443-14459, 10.1029/94jd00797, 1994.
Hudson, J. G., and Yum, S. S.: Cloud condensation nuclei spectra and polluted and clean clouds over the Indian Ocean, 107, INX2 21-21-INX22 21-12, 10.1029/2001jd000829, 2002.
IPCC: Climate change 2013: The physical science basis, Intergovernmental panel on Climate Change, Cambridge University Press, New York, USA, 571-740, 2013.
Jang, E., Park, K. T., Yoon, Y. J., Kim, T. W., Hong, S. B., Becagli, S., Traversi, R., Kim, J., and Gim, Y.: New particle formation events observed at the King Sejong Station, Antarctic Peninsula – Part 2: Link with the oceanic biological activities, Atmos. Chem. Phys., 19, 7595-7608, 10.5194/acp-19-7595-2019, 2019.
Jung, C. H., Yoon, Y. J., Kang, H. J., Gim, Y., Lee, B. Y., Ström, J., Krejci, R., and Tunved, P.: The seasonal characteristics of cloud condensation nuclei (CCN) in the arctic lower troposphere, Tellus B: Chemical and Physical Meteorology, 70, 1-13, 10.1080/16000889.2018.1513291, 2018.

Kalivitis, N., Kerminen, V. M., Kouvarakis, G., Stavroulas, I., Bougiatioti, A., Nenes, A., Manninen, H. E., Petäjä, T., Kulmala, M., and Mihalopoulos, N.: Atmospheric new particle formation as a source of CCN in the eastern Mediterranean marine boundary layer, Atmos. Chem. Phys., 15, 9203-9215, 10.5194/acp-15-9203-2015, 2015.

Kerminen, V.-M., Chen, X., Vakkari, V., Petäjä, T., Kulmala, M., and Bianchi, F.: Atmospheric new particle formation and growth: review of field observations, Environmental Research Letters, 13, 103003, 10.1088/1748-9326/aadf3c, 2018.

Kim, G., Cho, H.-j., Seo, A., Kim, D., Gim, Y., Lee, B. Y., Yoon, Y. J., and Park, K.: Comparison of Hygroscopicity, Volatility, and Mixing State of Submicrometer Particles between Cruises over the Arctic Ocean and the Pacific Ocean, Environmental Science & Technology, 49, 12024-12035, 10.1021/acs.est.5b01505, 2015.

Kim, J., Yoon, Y. J., Gim, Y., Kang, H. J., Choi, J. H., Park, K. T., and Lee, B. Y.: Seasonal variations in physical characteristics of aerosol particles at the King Sejong Station, Antarctic Peninsula, Atmos. Chem. Phys., 17, 12985-12999, 10.5194/acp-17-12985-2017, 2017.

Kim, J., Yoon, Y. J., Gim, Y., Choi, J. H., Kang, H. J., Park, K. T., Park, J., and Lee, B. Y.: New particle formation events observed at King Sejong Station, Antarctic Peninsula – Part 1: Physical characteristics and contribution to cloud condensation nuclei, Atmos. Chem. Phys., 19, 7583-7594, 10.5194/acp-19-7583-2019, 2019.

Kolesar, K. R., Cellini, J., Peterson, P. K., Jefferson, A., Tuch, T., Birmili, W., Wiedensohler, A., and Pratt, K. A.: Effect of Prudhoe Bay emissions on atmospheric aerosol growth events observed in Utqiaġvik (Barrow), Alaska, Atmospheric Environment, 152, 146-155, https://doi.org/10.1016/j.atmosenv. 2016.12.019, 2017.

Kulmala, M., Vehkamäki, H., Petäjä, T., Dal Maso, M., Lauri, A., Kerminen, V. M., Birmili, W., and McMurry, P. H.: Formation and growth rates of ultrafine atmospheric particles: a review of observations, Journal of Aerosol Science, 35, 143-176, https://doi.org/10.1016/j.jaerosci.2003.10.003, 2004.

Law, K. S., and Stohl, A.: Arctic Air Pollution: Origins and Impacts, Science, 315, 1537-1540, 10.1126/science.1137695, 2007.

Leaitch, W. R., Sharma, S., Huang, L., Toom-Sauntry, D., Chivulescu, A., Macdonald, A. M., von Salzen, K., Pierce, J. R., Bertram, A. K., Schroder, J. C., Shantz, N. C., Chang, R. Y.-W., and Norman, A.-L.: Dimethyl sulfide control of the clean summertime Arctic aerosol and cloud, Elem. Sci. Anth., 1, 000017, 10.12952/journal.elementa.000017, 2013.

Leck, C., Norman, M., Bigg, E. K., and Hillamo, R.: Chemical composition and sources of the high Arctic aerosol relevant for cloud formation, 107, AAC 1-1-AAC 1-17, 10.1029/2001jd001463, 2002.

Levasseur, M.: Impact of Arctic meltdown on the microbial cycling of sulphur, Nature Geoscience, 6, 691, 10.1038/ngeo1910, 2013.

Lindwall, F., Schollert, M., Michelsen, A., Blok, D., and Rinnan, R.: Fourfold higher tundra volatile emissions due to arctic summer warming, 121, 895-902, 10.1002/2015jg003295, 2016.

Mann, P. J., Spencer, R. G. M., Hernes, P. J., Six, J., Aiken, G. R., Tank, S. E., McClelland, J. W., Butler, K. D., Dyda, R. Y., and Holmes, R. M.: Pan-Arctic Trends in Terrestrial Dissolved Organic Matter from Optical Measurements, 4, 10.3389/feart.2016.00025, 2016.

Martin, M., Chang, R. Y. W., Sierau, B., Sjogren, S., Swietlicki, E., Abbatt, J. P. D., Leck, C., and Lohmann, U.: Cloud condensation nuclei closure study on summer arctic aerosol, Atmos. Chem. Phys., 11, 11335-11350, 10.5194/acp-11-11335-2011, 2011.

Massicotte, P., Asmala, E., Stedmon, C., and Markager, S.: Global distribution of dissolved organic matter along the aquatic continuum: Across rivers, lakes and oceans, Science of The Total Environment, 609, 180-191, https://doi.org/10.10 16/j.scitotenv.2017.07.076, 2017.

Mauritsen, T., Sedlar, J., Tjernström, M., Leck, C., Martin, M., Shupe, M., Sjogren, S., Sierau, B., Persson, P. O. G., Brooks, I. M., and Swietlicki, E.: An Arctic CCN-limited cloud-aerosol regime, Atmos. Chem. Phys., 11, 165-173, 10.5194/acp-11-165-2011, 2011.

Merikanto, J., Spracklen, D. V., Mann, G. W., Pickering, S. J., and Carslaw, K. S.: Impact of nucleation on global CCN, Atmos. Chem. Phys., 9, 8601-8616, 10.5194/acp-9-8601-2009, 2009.
Mungall, E. L., Croft, B., Lizotte, M., Thomas, J. L., Murphy, J. G., Levasseur, M., Martin, R. V., Wentzell, J. J. B., Liggio, J., and Abbatt, J. P. D.: Dimethyl sulfide in the summertime Arctic atmosphere: measurements and source sensitivity simulations, Atmos. Chem. Phys., 16, 6665-6680, 10.5194/acp-16-6665-2016, 2016.
Németh, Z., and Salma, I.: Spatial extension of nucleating air masses in the Carpathian Basin, Atmos. Chem. Phys., 14, 8841-8848, 10.5194/acp-14-8841-2014, 2014.
Nguyen, Q. T., Glasius, M., Sørensen, L. L., Jensen, B., Skov, H., Birmili, W., Wiedensohler, A., Kristensson, A., Nøjgaard, J. K., and Massling, A.: Seasonal variation of atmospheric particle number concentrations, new particle formation and atmospheric oxidation capacity at the high Arctic site Villum Research Station, Station Nord, Atmos. Chem. Phys., 16, 11319-11336, 10.5194/acp-16-11319-2016, 2016.
O'Dowd, C., Ceburnis, D., Ovadnevaite, J., Vaishya, A., Rinaldi, M., and Facchini, M. C.: Do anthropogenic, continental or coastal aerosol sources impact on a marine aerosol signature at Mace Head?, Atmos. Chem. Phys., 14, 10687-10704, 10.5194/acp-14-10687-2014, 2014.
O'Dowd, C. D., Jimenez, J. L., Bahreini, R., Flagan, R. C., Seinfeld, J. H., Hämeri, K., Pirjola, L., Kulmala, M., Jennings, S. G., and Hoffmann, T.: Marine aerosol formation from biogenic iodine emissions, Nature, 417, 632, 10.1038/nature00775, 2002.
Oziel, L., Neukermans, G., Ardyna, M., Lancelot, C., Tison, J.-L., Wassmann, P., Sirven, J., Ruiz-Pino, D., and Gascard, J.-C.: Role for Atlantic inflows and sea ice loss on shifting phytoplankton blooms in the Barents Sea, 122, 5121-5139, 10.1002/2016jc012582, 2017.
Pang, X., Pu, J., Zhao, X., Ji, Q., Qu, M., and Cheng, Z.: Comparison between AMSR2 Sea Ice Concentration Products and Pseudo-Ship Observations of the Arctic and Antarctic Sea Ice Edge on Cloud-Free Days, 10, 317, 2018.
Park, J., Dall'Osto, M., Park, K., Kim, J.-H., Park, J., Park, K.-T., Hwang, C. Y., Jang, G. I., Gim, Y., Kang, S., Park, S., Jin, Y. K., Yum, S. S., Simó, R., and Yoon, Y. J.: Arctic Primary Aerosol Production Strongly Influenced by Riverine Organic Matter, Environmental Science & Technology, 53, 8621-8630, 10.1021/acs.est.9b03399, 2019.
Park, K.-T., Lee, K., Kim, T.-W., Yoon, Y. J., Jang, E.-H., Jang, S., Lee, B.-Y., and Hermansen, O.: Atmospheric DMS in the Arctic Ocean and Its Relation to Phytoplankton Biomass, 32, 351-359, 10.1002/2017gb005805, 2018.
Park, K. T., Jang, S., Lee, K., Yoon, Y. J., Kim, M. S., Park, K., Cho, H. J., Kang, J. H., Udisti, R., Lee, B. Y., and Shin, K. H.: Observational evidence for the formation of DMS-derived aerosols during Arctic phytoplankton blooms, Atmos. Chem. Phys., 17, 9665-9675, 10.5194/acp-17-9665-2017, 2017.
Peñuelas, J., and Staudt, M.: BVOCs and global change, Trends in Plant Science, 15, 133-144, https://doi.org/10.1016/j.tplants.2009.12.005, 2010.
Peters, G. P., Nilssen, T. B., Lindholt, L., Eide, M. S., Glomsrød, S., Eide, L. I., and Fuglestvedt, J. S.: Future emissions from shipping and petroleum activities in the Arctic, Atmos. Chem. Phys., 11, 5305-5320, 10.5194/acp-11-5305-2011, 2011.
Peterson, B. J., Holmes, R. M., McClelland, J. W., Vörösmarty, C. J., Lammers, R. B., Shiklomanov, A. I., Shiklomanov, I. A., and Rahmstorf, S.: Increasing River Discharge to the Arctic Ocean, Science, 298, 2171-2173, 10.1126/science.1077445, 2002.
Pierce, J. R., Leaitch, W. R., Liggio, J., Westervelt, D. M., Wainwright, C. D., Abbatt, J. P. D., Ahlm, L., Al-Basheer, W., Cziczo, D. J., Hayden, K. L., Lee, A. K. Y., Li, S. M., Russell, L. M., Sjostedt, S. J., Strawbridge, K. B., Travis, M., Vlasenko, A., Wentzell, J. J. B., Wiebe, H. A., Wong, J. P. S., and Macdonald, A. M.: Nucleation and condensational growth to CCN sizes during a sustained pristine biogenic SOA event in a forested mountain valley, Atmos. Chem. Phys., 12, 3147-3163, 10.5194/acp-12-3147-2012, 2012.
Pierce, J. R., Westervelt, D. M., Atwood, S. A., Barnes, E. A., and Leaitch, W. R.: New-particle

formation, growth and climate-relevant particle production in Egbert, Canada: analysis from 1 year of size-distribution observations, Atmos. Chem. Phys., 14, 8647-8663, 10.5194/acp-14-8647-2014, 2014.
Potosnak, M. J., Baker, B. M., LeStourgeon, L., Disher, S. M., Griffin, K. L., Bret-Harte, M. S., and Starr, G.: Isoprene emissions from a tundra ecosystem, Biogeosciences, 10, 871-889, 10.5194/bg-10-871-2013, 2013.
Quinn, P. K., and Bates, T. S.: The case against climate regulation via oceanic phytoplankton sulphur emissions, Nature, 480, 51-56, 10.1038/nature10580, 2011.
Quinn, P. K., Collins, D. B., Grassian, V. H., Prather, K. A., and Bates, T. S.: Chemistry and Related Properties of Freshly Emitted Sea Spray Aerosol, Chemical Reviews, 115, 4383-4399, 10.1021/cr500713g, 2015.
Raso, A. R. W., Custard, K. D., May, N. W., Tanner, D., Newburn, M. K., Walker, L., Moore, R. J., Huey, L. G., Alexander, L., Shepson, P. B., and Pratt, K. A.: Active molecular iodine photochemistry in the Arctic, Proceedings of the National Academy of Sciences, 114, 10053-10058, 10.1073/pnas.1702803114, 2017.
Rose, C., Sellegri, K., Moreno, I., Velarde, F., Ramonet, M., Weinhold, K., Krejci, R., Andrade, M., Wiedensohler, A., Ginot, P., and Laj, P.: CCN production by new particle formation in the free troposphere, Atmos. Chem. Phys., 17, 1529-1541, 10.5194/acp-17-1529-2017, 2017.
Schmale, J., Arnold, S. R., Law, K. S., Thorp, T., Anenberg, S., Simpson, W. R., Mao, J., and Pratt, K. A.: Local Arctic Air Pollution: A Neglected but Serious Problem, 6, 1385-1412, 10.1029/2018ef000952, 2018a.
Schmale, J., Henning, S., Decesari, S., Henzing, B., Keskinen, H., Sellegri, K., Ovadnevaite, J., Pöhlker, M. L., Brito, J., Bougiatioti, A., Kristensson, A., Kalivitis, N., Stavroulas, I., Carbone, S., Jefferson, A., Park, M., Schlag, P., Iwamoto, Y., Aalto, P., Äijälä, M., Bukowiecki, N., Ehn, M., Frank, G., Fröhlich, R., Frumau, A., Herrmann, E., Herrmann, H., Holzinger, R., Kos, G., Kulmala, M., Mihalopoulos, N., Nenes, A., O'Dowd, C., Petäjä, T., Picard, D., Pöhlker, C., Pöschl, U., Poulain, L., Prévôt, A. S. H., Swietlicki, E., Andreae, M. O., Artaxo, P., Wiedensohler, A., Ogren, J., Matsuki, A., Yum, S. S., Stratmann, F., Baltensperger, U., and Gysel, M.: Long-term cloud condensation nuclei number concentration, particle number size distribution and chemical composition measurements at regionally representative observatories, Atmos. Chem. Phys., 18, 2853-2881, 10.5194/acp-18-2853-2018, 2018b.
Schollert, M., Burchard, S., Faubert, P., Michelsen, A., and Rinnan, R. J. P. B.: Biogenic volatile organic compound emissions in four vegetation types in high arctic Greenland, 37, 237-249, 10.1007/s00300-013-1427-0, 2014.
Sellegri, K., O'Dowd, C. D., Yoon, Y. J., Jennings, S. G., and Leeuw, G. d.: Surfactants and submicron sea spray generation, Journal of Geophysical Research: Atmospheres, 111, doi:10.1029/2005JD006658, 2006.
Shen, Y., Fichot, C., and Benner, R.: Dissolved organic matter composition and bioavailability reflect ecosystem productivity in the Western Arctic Ocean, 2012.
Shiklomanov, I. A., Shiklomanov, A. I., Lammers, R. B., Peterson, B. J., and Vorosmarty, C. J.: The Dynamics of River Water Inflow to the Arctic Ocean, in: The Freshwater Budget of the Arctic Ocean, edited by: Lewis, E. L., Jones, E. P., Lemke, P., Prowse, T. D., and Wadhams, P., Springer Netherlands, Dordrecht, 281-296, 2000.
Spracklen, D. V., Carslaw, K. S., Kulmala, M., Kerminen, V.-M., Sihto, S.-L., Riipinen, I., Merikanto, J., Mann, G. W., Chipperfield, M. P., Wiedensohler, A., Birmili, W., and Lihavainen, H.: Contribution of particle formation to global cloud condensation nuclei concentrations, Geophysical Research Letters, 35, doi:10.1029/2007GL033038, 2008.
Steinke, M., Hodapp, B., Subhan, R., Bell, T. G., and Martin-Creuzburg, D.: Flux of the biogenic volatiles isoprene and dimethyl sulfide from an oligotrophic lake, Scientific Reports, 8, 630, 10.1038/s41598-017-18923-5, 2018.
Stier, P., Seinfeld, J. H., Kinne, S., and Boucher, O.: Aerosol absorption and radiative forcing, Atmos.

Chem. Phys., 7, 5237-5261, 10.5194/acp-7-5237-2007, 2007.
Stroeve, J. C., Serreze, M. C., Holland, M. M., Kay, J. E., Malanik, J., and Barrett, A. P.: The Arctic's rapidly shrinking sea ice cover: a research synthesis, Climatic Change, 110, 1005-1027, 10.1007/s10584-011-0101-1, 2012.
Ström, J., Umegård, J., Tørseth, K., Tunved, P., Hansson, H. C., Holmén, K., Wismann, V., Herber, A., and König-Langlo, G.: One year of particle size distribution and aerosol chemical composition measurements at the Zeppelin Station, Svalbard, March 2000–March 2001, Physics and Chemistry of the Earth, Parts A/B/C, 28, 1181-1190, https://doi.org/10.1016/j.pce.2003.08.058, 2003.
Suni, T., Kulmala, M., Hirsikko, A., Bergman, T., Laakso, L., Aalto, P. P., Leuning, R., Cleugh, H., Zegelin, S., Hughes, D., van Gorsel, E., Kitchen, M., Vana, M., Hõrrak, U., Mirme, S., Mirme, A., Sevanto, S., Twining, J., and Tadros, C.: Formation and characteristics of ions and charged aerosol particles in a native Australian Eucalypt forest, Atmos. Chem. Phys., 8, 129-139, 10.5194/acp-8-129-2008, 2008.
Svenningsson, B., Arneth, A., Hayward, S., Holst, T., Massling, A., Swietlicki, E., Hirsikko, A., Junninen, H., Riipinen, I., Vana, M., Maso, M. D., Hussein, T., and Kulmala, M.: Aerosol particle formation events and analysis of high growth rates observed above a subarctic wetland–forest mosaic, Tellus B: Chemical and Physical Meteorology, 60, 353-364, 10.1111/j.1600-0889.2008.00351.x, 2008.
TAPE, K., STURM, M., and RACINE, C.: The evidence for shrub expansion in Northern Alaska and the Pan-Arctic, 12, 686-702, 10.1111/j.1365-2486.2006.01128.x, 2006.
Tremblay, S., Picard, J.-C., Bachelder, J. O., Lutsch, E., Strong, K., Fogal, P., Leaitch, W. R., Sharma, S., Kolonjari, F., Cox, C. J., Chang, R. Y.-W., and Hayes, P. L.: Characterization of aerosol growth events over Ellesmere Island during the summers of 2015 and 2016, Atmos. Chem. Phys., 19, 5589–5604, https://doi.org/10.5194/acp-19-5589-2019, 2019.
Tunved, P., Ström, J., and Krejci, R.: Arctic aerosol life cycle: linking aerosol size distributions observed between 2000 and 2010 with air mass transport and precipitation at Zeppelin station, Ny-Ålesund, Svalbard, Atmos. Chem. Phys., 13, 3643-3660, 10.5194/acp-13-3643-2013, 2013.
Twomey, S.: Pollution and the planetary albedo, Atmospheric Environment (1967), 8, 1251-1256, https://doi.org/10.1016/0004-6981(74)90004-3, 1974.
Väänänen, R., Kyrö, E. M., Nieminen, T., Kivekäs, N., Junninen, H., Virkkula, A., Dal Maso, M., Lihavainen, H., Viisanen, Y., Svenningsson, B., Holst, T., Arneth, A., Aalto, P. P., Kulmala, M., and Kerminen, V. M.: Analysis of particle size distribution changes between three measurement sites in northern Scandinavia, Atmos. Chem. Phys., 13, 11887-11903, 10.5194/acp-13-11887-2013, 2013.
Vana, M., Kulmala, M., Dal Maso, M., Hõrrak, U., and Tamm, E.: Comparative study of nucleation mode aerosol particles and intermediate air ions formation events at three sites, 109, 10.1029/2003jd004413, 2004.
Vehkamäki, H., Dal Maso, M., Hussein, T., Flanagan, R., Hyvärinen, A., Lauros, J., Merikanto, P., Mönkkönen, M., Pihlatie, K., Salminen, K., Sogacheva, L., Thum, T., Ruuskanen, T. M., Keronen, P., Aalto, P. P., Hari, P., Lehtinen, K. E. J., Rannik, Ü., and Kulmala, M.: Atmospheric particle formation events at Värriö measurement station in Finnish Lapland 1998-2002, Atmos. Chem. Phys., 4, 2015-2023, 10.5194/acp-4-2015-2004, 2004.
Wang, M., and Overland, J. E.: A sea ice free summer Arctic within 30 years?, Geophysical Research Letters, 36, doi:10.1029/2009GL037820, 2009.
Watson, J. G., Chow, J. C., Sodeman, D. A., Lowenthal, D. H., Chang, M. C. O., Park, K., and Wang, X.: Comparison of four scanning mobility particle sizers at the Fresno Supersite, Particuology, 9, 204-209, 2011.
Westervelt, D. M., Pierce, J. R., and Adams, P. J.: Analysis of feedbacks between nucleation rate, survival probability and cloud condensation nuclei formation, Atmos. Chem. Phys., 14, 5577-5597, 10.5194/acp-14-5577-2014, 2014.

Willis, M. D., Burkart, J., Thomas, J. L., Köllner, F., Schneider, J., Bozem, H., Hoor, P. M., Aliabadi, A. A., Schulz, H., Herber, A. B., Leaitch, W. R., and Abbatt, J. P. D.: Growth of nucleation mode particles in the summertime Arctic: a case study, Atmos. Chem. Phys., 7663-7679, 10.5194/acp-16-7663-2016, 2016.

Willis, M. D., Leaitch, W. R., and Abbatt, J. P. D.: Processes Controlling the Composition and Abundance of Arctic Aerosol, 56, 621-671, 10.1029/2018rg000602, 2018.

Yum, S. S., Hudson, J. G., and Xie, Y.: Comparisons of cloud microphysics with cloud condensation nuclei spectra over the summertime Southern Ocean, 103, 16625-16636, 10.1029/98jd01513, 1998.

Zhang, R., Khalizov, A., Wang, L., Hu, M., and Xu, W.: Nucleation and Growth of Nanoparticles in the Atmosphere, Chemical Reviews, 112, 1957-2011, 10.1021/cr2001756, 2012.

Ziemba, L. D., Dibb, J. E., Griffin, R. J., Huey, L. G., and Beckman, P.: Observations of particle growth at a remote, Arctic site, Atmos. Environ., 44, 1649–1657, https://doi.org/10.1016/j.atmosenv.2010.01.032, 2010.

Table 1. A summary of meteorology, total number concentrations of particles (measured with TSI 3776 CPC, TSI 3772 CPC, Standard SMPS, nano SMPS), growth rate (GR), and condensation sink (CS) for the three selected periods. The $CN_{2.5}$ and CN_{10} represents the total number concentration of particles larger than 2.5 nm and 10 nm, respectively. The N_{NUC}, N_{AIT}, N_{ACC}, and N_{OPS} represents total aerosol nucleation-mode (3 − 20 nm), Aitken-mode (20 − 100 nm), accumulation-mode (100 − 300 nm), and coarse-mode (> 300 nm from OPS) number concentrations.

	Arctic Marine	Arctic Terrestrial	Pacific Ocean
Periods	9/02/2017−9/05/2017, 9/10/2017−9/12/2017	9/13/2017−9/17/2017	9/21/2017−9/23/2017
Wind speed (m s^{-1})	6.1 ± 6.0	8.7 ± 5.7	8.4 ± 4.3
Wind direction (°)	352.3 ± 38.7	344.7 ± 28.1	338.3 ± 23.0
$CN_{2.5}$ (cm^{-3})	413 ± 442	1622 ± 1450	397 ± 185
CN_{10} (cm^{-3})	414 ± 452	1396 ± 1279	384 ± 86
$CN_{2.5-10}$ (cm^{-3})	62 ± 130	263 ± 318	35 ± 195
N_{NUC} (cm^{-3})	118 ± 198	350 ± 393	46 ± 103
N_{AIT} (cm^{-3})	108 ± 132	405 ± 425	116 ± 93
N_{ACC} (cm^{-3})	19 ± 14	33 ± 20	95 ± 30
N_{OPS} (cm^{-3})	2 ± 2	3 ± 2	11 ± 6
GR (nm h^{-1})	0.4 ± 0.3	0.8 ± 0.2	-
CS (h^{-1})	0.5 ± 0.4	0.9 ± 0.5	2.1 ± 0.7

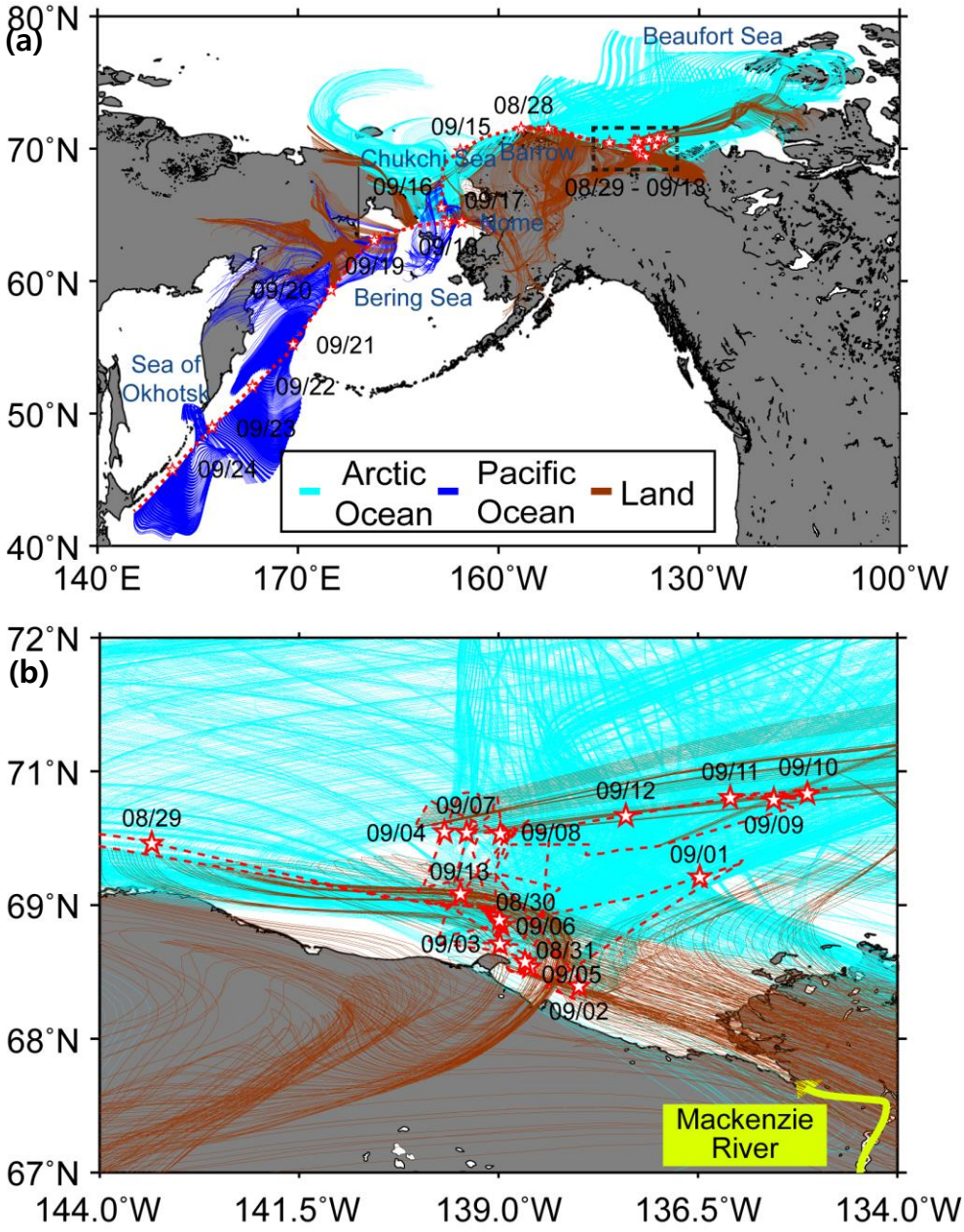

Figure 1. Ship tracks across (a) the Arctic (8/28/2017−9/18/2017) and Pacific Oceans (9/18/2017−9/25/2017) and (b) zoom into the dotted black square region in Fig. 1a. A dotted red line including star symbols represents ship tracks during the entire cruise. The star symbols represent the daily ship location at midnight. Light blue, blue and brown lines denote the 2-day air mass trajectories categorized into three main domains such as Arctic Ocean, Pacific Ocean, and land, respectively.

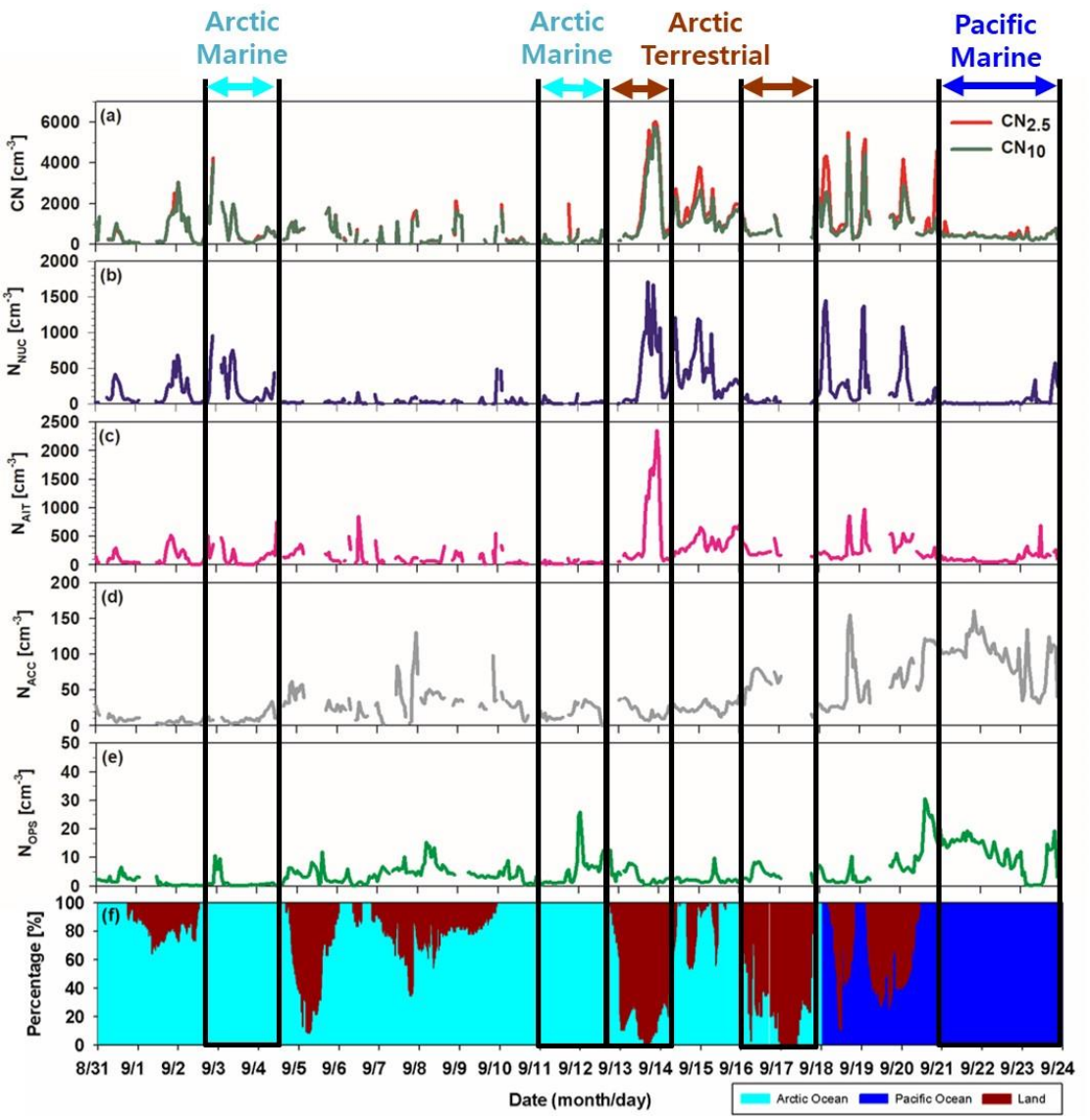

Figure 2. Time series of the 1 hour average (a) total aerosol ($CN_{2.5}$ and CN_{10}), (b) nucleation-mode (3 − 20 nm) (N_{NUC}), (c) Aitken-mode (20 − 100 nm) (N_{AIT}), (d) accumulation-mode (100 − 300 nm) (N_{ACC}), (e) coarse-mode (> 300 nm from OPS) (N_{OPS}) number concentrations, and (f) the residence time of air masses that passed over the Arctic Ocean, Pacific Ocean, and land. The $CN_{2.5}$ and CN_{10} represent total number concentration of particles larger than 2.5 and 10 nm, respectively.

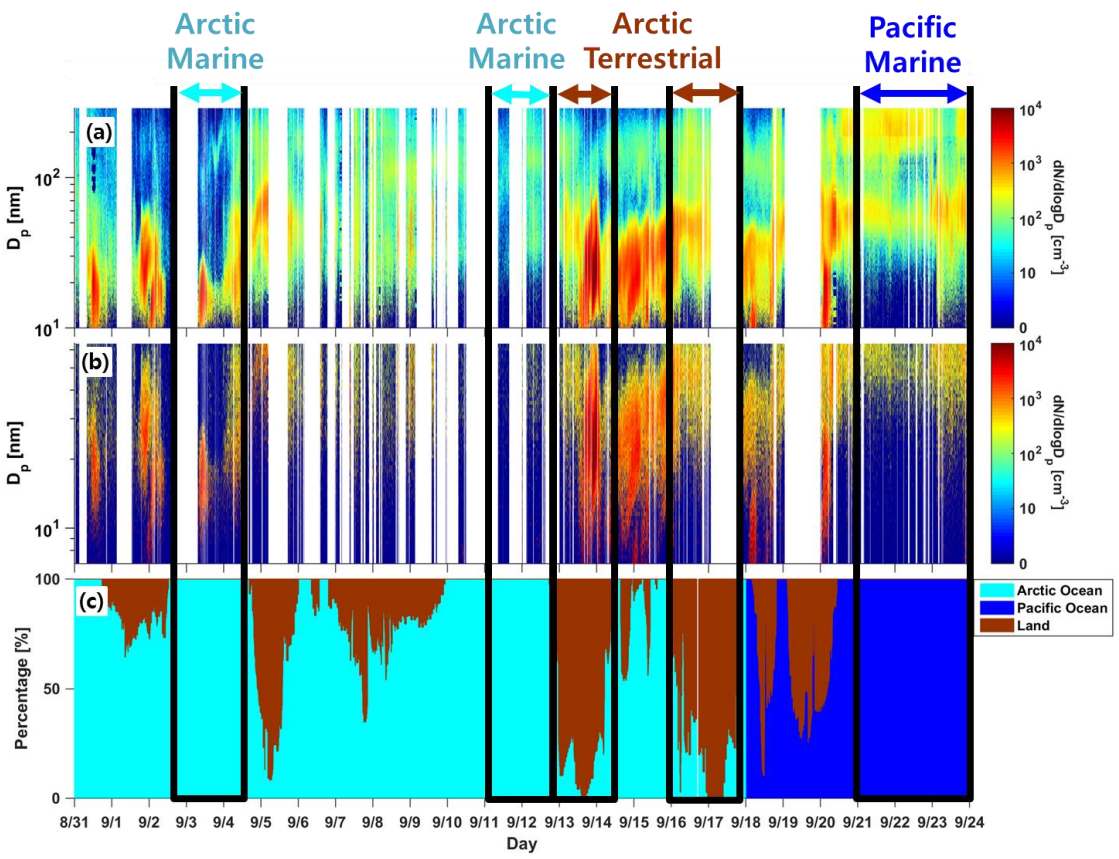

Figure 3. Contour plots of the size distributions measured using (a) standard and (b) nano SMPS and (c) the residence time of air masses that passed over the Arctic Ocean, Pacific Ocean, and land throughout the sampling periods.

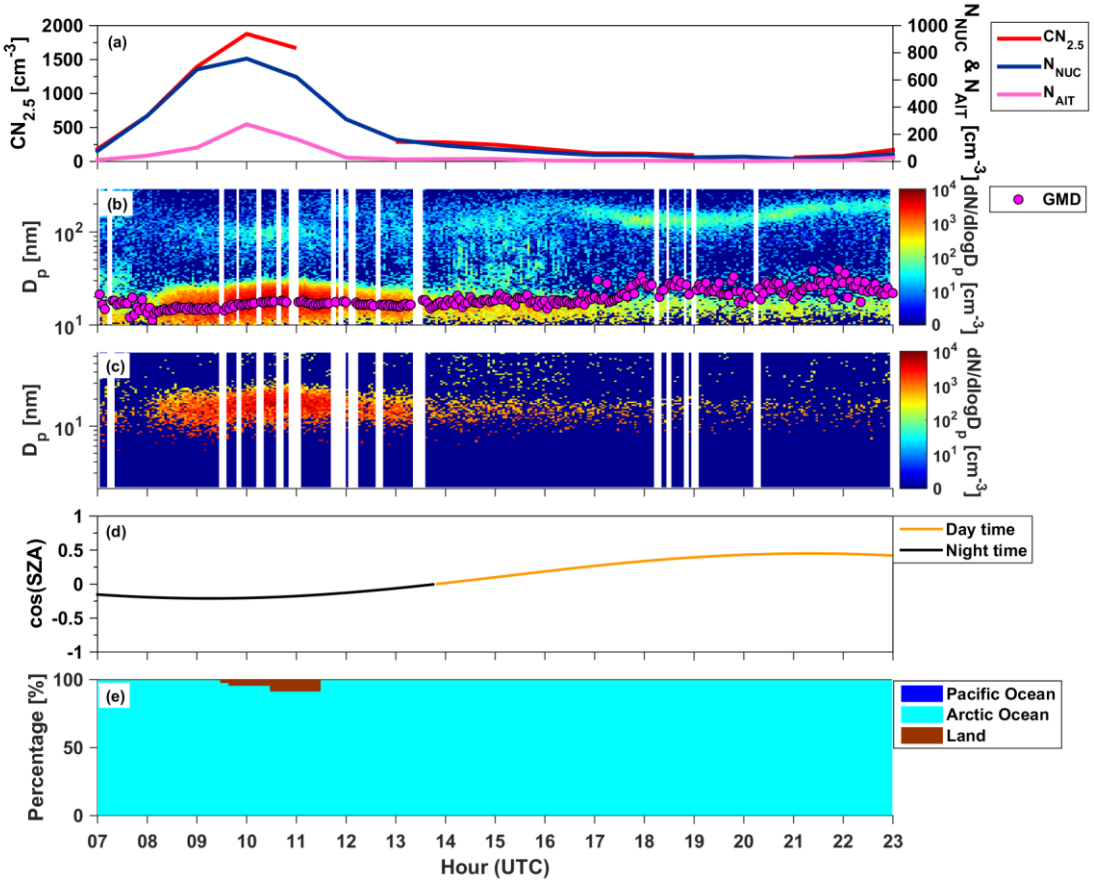

Figure 4. Example of a case-I event observed on 3 September 2017. From top to bottom, the parameters are: (a) the total number concentration of particles smaller than 2.5 nm, nucleation-mode particles, and Aitken-mode particles; (b) a time series of the standard SMPS size distribution and GMD; (c) a time series of the nano SMPS size; (d) Cosine values of solar zenith angle; (e) the residence time of air masses that passed over the ocean, land, and sea-ice areas.

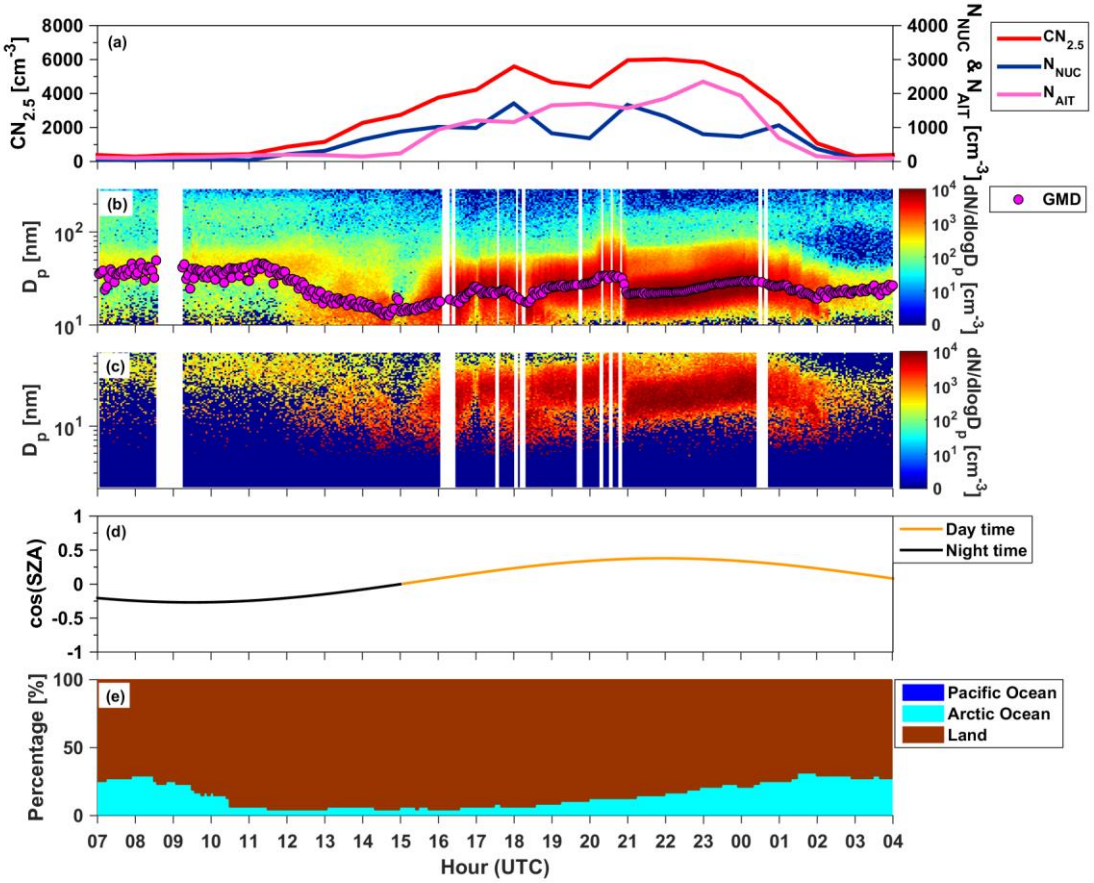

Figure 5. Example of a case II event that was observed on September 13−14, 2017. From top to bottom, the parameters are: (a) the total number concentration of particles smaller than 2.5 nm, nucleation-mode particles, and Aitken-mode particles; (b) a time series of the standard SMPS size distribution and GMD; (c) a time series of the nano SMPS size; (d) cosine values of solar zenith angle; (e) the residence time of air masses that passed over the ocean, land, and sea-ice areas.

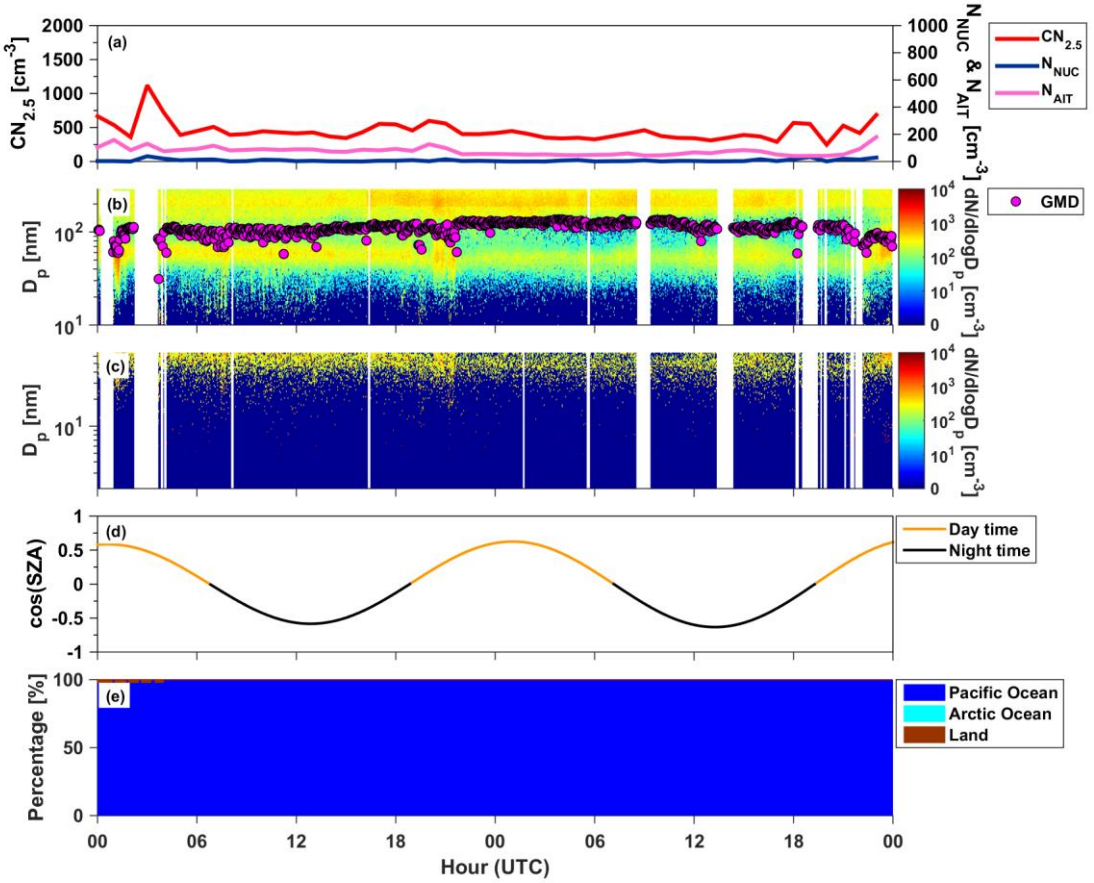

Figure 6. Example of a case III event that was observed on September 21−22 2017. From top to bottom, the parameters are: (a) the total number concentration of particles smaller than 2.5 nm, nucleation-mode particles, and Aitken-mode particles; (b) a time series of the standard SMPS size distribution and GMD; (c) a time series of the nano SMPS size; (d) cosine values of solar zenith angle; (e) the residence time of air masses that passed over the ocean, land, and sea-ice areas.

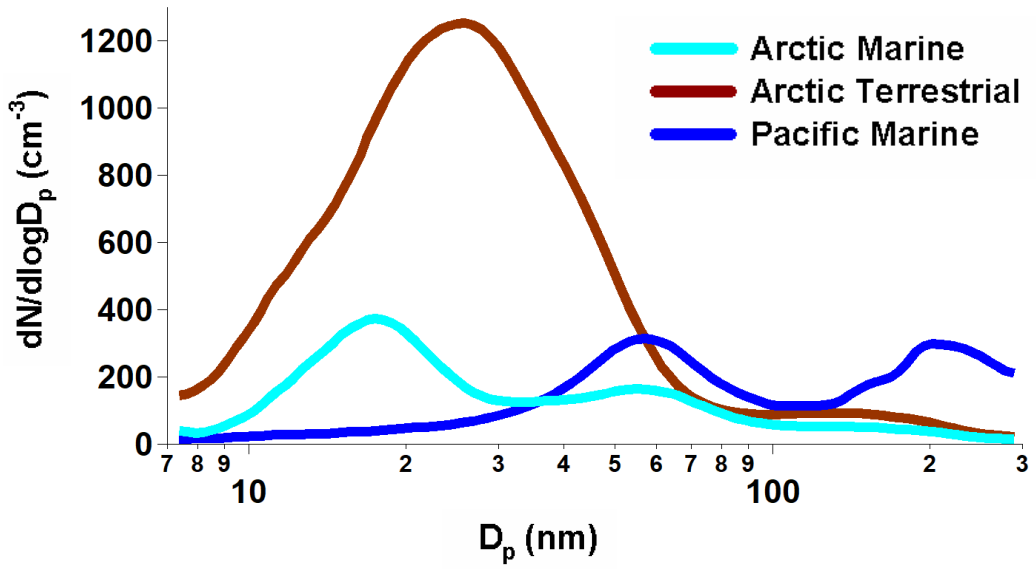

Figure 7. Average size distributions of aerosol particles for Arctic marine, Arctic terrestrial and Pacific marine air masses

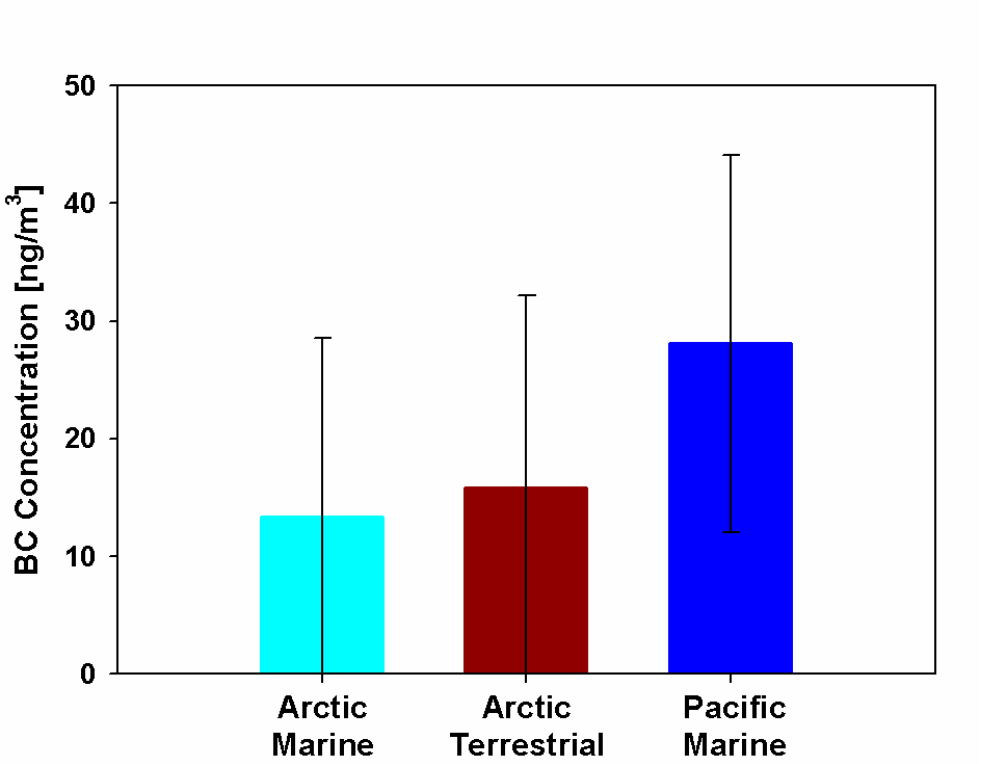

Figure 8. Average mass concentrations of black carbon for each air mass.

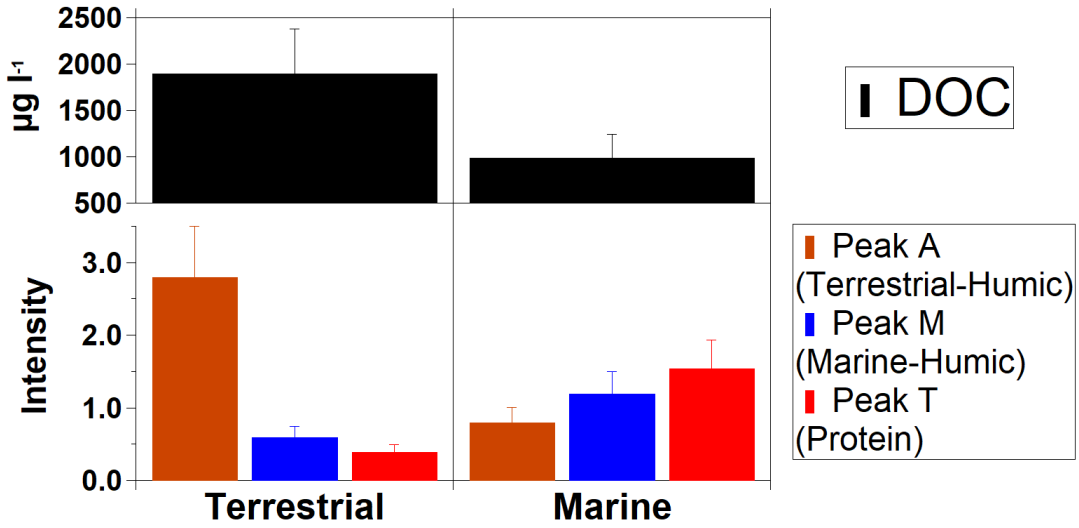

Figure 9. Average DOC concentrations for surface seawater samples collected during this cruise, simultaneously during the atmospheric measurements herein reported. Peak A, M, and T represent terrestrial-humic substances, marine-fulvic substances, and protein, respectively.

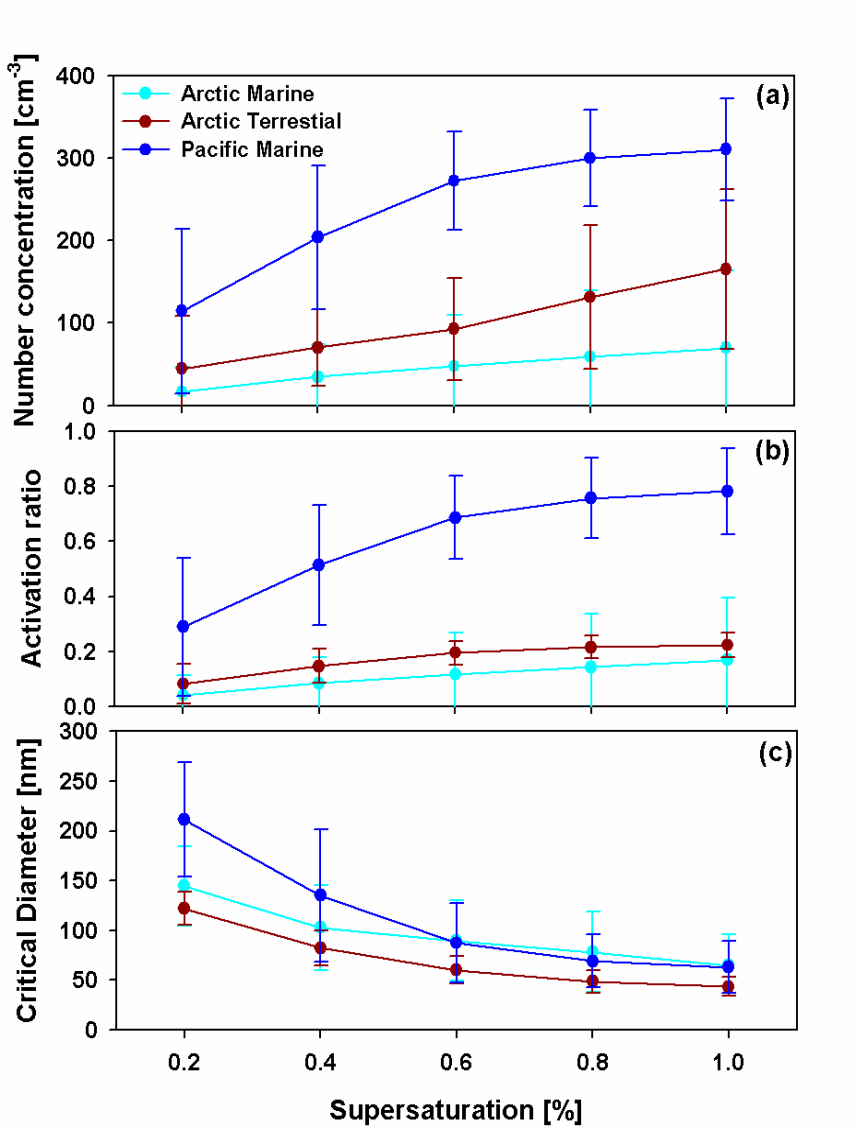

Figure 10. Comparisons of (a) CCN number concentrations, (b) CCN activity, and (c) critical diameter for Arctic marine, Arctic terrestrial and Pacific marine air masses under different supersaturation conditions. The error bars represent a standard deviation.